

# Footprints of New Physics in the angular distribution of $B_c \rightarrow D_s^*(\rightarrow D_s\gamma, (D_s\pi))\ell^+\ell^-$ decays

Marwah Zaki\*, M. Ali Paracha<sup>†</sup> and Faisal Munir Bhutta<sup>‡</sup>

Department of Physics, School of Natural Sciences, National University of  
Sciences and Technology, H-12, Islamabad, Pakistan

August 1, 2023

## Abstract

We investigate the angular decay distribution of the four-fold  $B_c \rightarrow D_s^*(\rightarrow D_s\gamma)\mu^+\mu^-$ , and  $B_c \rightarrow D_s^*(\rightarrow D_s\pi)\mu^+\mu^-$  decays that proceed through  $b \rightarrow s\mu^+\mu^-$  quark level transition. We use the model independent effective Hamiltonian with vector and axial vector new physics operators to formulate the angular observables and study the implications of different latest new physics scenarios, taken from the global fits to all the  $b \rightarrow s$  data, on these observables. We also give Standard Model and new physics predictions of several observables such as differential branching ratios, forward backward asymmetry, longitudinal polarization fraction of  $D_s^*$ , and the unpolarized and polarized lepton flavor universality violating ratios. Future measurements of the predicted angular observables, both at current and future high energy colliders, will add to the useful complementary data required to clarify the structure of new physics in  $b \rightarrow s\ell\ell$  neutral current decays.

## 1 Introduction

High Energy Physics community has put a lot of effort over the past decade in searching the new physics (NP) via exclusive decays of  $B$  meson based on flavor changing neutral (FCNC) transitions, in particular  $b \rightarrow s\ell^+\ell^-$  mode. These FCNC transitions occur only at loop level in the Standard Model (SM) and hence provide a fertile ground to investigate NP as well as the SM parameters.  $B \rightarrow K^*(\rightarrow K\pi)\mu\mu$ , and  $B \rightarrow K\mu\mu$  decays and their angular distributions have been studied in great detail at the LHCb experiments [1–7]. From the angular distributions of such decays, new set of observables have been constructed which are free from the Cabibbo-Kobayashi-Maskawa (CKM) uncertainties, and therefore furnish a complementary way to diagnose the status of NP [8]. However the main hindrance to chalk out the status of NP via angular observables are the hadronic uncertainties. There is an improvement in controlling the uncertainties in the hadronic matrix elements of local quark operators and in few cases the uncertainty is about 10%. On the other hand, the matrix element of the non-local quark operators appearing from the coupling of charmonium states, remains a daunting task to

---

\*mzaki.msphy20sns@student.nust.edu.pk

†aliparacha@sns.nust.edu.pk

‡faisal.munir@sns.nust.edu.pk

handle [9]. Both of the above mentioned hadronic uncertainties are almost negligibly small in the ratios  $R_{K^{(*)}} = \frac{\mathcal{B}(B \rightarrow K^{(*)}\mu^+\mu^-)}{\mathcal{B}(B \rightarrow K^{(*)}e^+e^-)}$  [10]. Recently the updated measurements of these observables  $R_K$ , and  $R_{K^*}$  [11, 12], have put stringent constraints on the NP couplings and the NP models.

Among several  $b \rightarrow s\mu\mu$  observables, showing deviations from the SM predictions, there are branching fractions of  $B \rightarrow K\mu^+\mu^-$  [13],  $B \rightarrow K^*\mu^+\mu^-$  [13–15], and  $B_s \rightarrow \phi\mu^+\mu^-$  [16, 17] decays. The values of these branching fractions are found to be on the lower side as compared to their SM predictions. Also, in angular observables,  $P'_5$  observable in the  $B^0 \rightarrow K^{*0}\mu^+\mu^-$  decay, [18, 19], has shown mismatch from the SM values. For instance, ATLAS [20], and LHCb [1, 2], measured the value of  $P'_5$  in the kinematical region  $4.0 < q^2 < 6.0 \text{ GeV}^2$  and found departure from the SM value to be more than  $3\sigma$  [21]. Furthermore Belle [22, 23] and CMS [24] measured the value of  $P'_5$  for the same decay mode in  $q^2$  bin  $4.0 < q^2 < 8.0 \text{ GeV}^2$  and  $6.0 < q^2 < 8.68 \text{ GeV}^2$  respectively. Belle measurement shows the deviation of  $2.6\sigma$  from the SM prediction and CMS measurement shows a discrimination of  $1\sigma$  from the SM value.

Considering all the  $b \rightarrow s$  data, including the above mentioned, several model independent global fit analyses [25–42] have been performed with NP present only in the muon sector, that found two simple one-dimensional (1D) NP scenarios (S1)  $C_{9\mu}^{\text{NP}}$  or (S2)  $C_{9\mu}^{\text{NP}} = -C_{10\mu}^{\text{NP}}$ , which give better fit to all the data, with preferences reaching  $\approx 5 - 6\sigma$  compared to the SM. Interestingly, if global fits predict the NP effects being present in the observables of  $B \rightarrow K^{(*)}\mu^+\mu^-$  and  $B_s \rightarrow \phi\mu^+\mu^-$  decay modes, following  $b \rightarrow s\mu^+\mu^-$  transition, then it is worth wondering that similar NP effects should also emerge in the observables of other complementary semileptonic decay modes followed by the same quark level transition. In this context, different complementary decay modes  $B \rightarrow K_1\mu^+\mu^-$  [43, 44],  $B \rightarrow K_2^*\mu^+\mu^-$  [45, 46],  $B_s \rightarrow f_2'\mu^+\mu^-$  [46, 47], and  $B_c \rightarrow D_s^{(*)}\mu^+\mu^-$  [48, 49] have been investigated both in model independent approach and the specific NP models. For example, in Ref. [48],  $B_c \rightarrow D_s^{(*)}\mu^+\mu^-$  decay observables have been investigated model independently with various 1D and 2D NP scenarios whereas the authors of Ref. [49] analyzed the  $B_c \rightarrow D_s^{(*)}\mu^+\mu^-$ , and  $B_c \rightarrow D_s^{(*)}\nu\bar{\nu}$  decays in a  $Z'$  and leptoquark models.

In this work, we use the model independent effective Hamiltonian in the presence of only vector and axial vector NP operators and perform the four-fold angular analysis of  $B_c \rightarrow D_s^*(\rightarrow D_s\gamma, D_s\pi)\mu\mu$  decays using the relativistic quark model (RQM) form factors in the low energy  $q^2$  range. For the decay channels  $D_s^* \rightarrow D_s\gamma$  the probability is 93%, and the probability of the channel  $D_s^* \rightarrow D_s\pi$  is 5%. As our NP extensions cater both new vector and axial vector couplings, therefore for the NP scenarios, we choose the best fit values of NP couplings in different 1D and 2D scenarios, from the recent global fit analysis [42]. We give the predictions of different physical observables such as differential branching fractions, forward-backward asymmetry, longitudinal helicity fraction of  $D_s^*$  meson, lepton flavor universality violating (LFUV) ratios, when  $D_s^*$  meson is longitudinally and transversely polarized and the individual angular observables within the SM and in different NP scenarios.

The organization of the paper is as follows. In section 2, we start with the general effective Hamiltonian, for  $b \rightarrow s\mu\mu$  transition, in the presence of vector and axial vector NP operators after which we express the matrix elements in terms of form factors for  $B_c \rightarrow D_s^*\mu^+\mu^-$  decay. Further, the helicity formalism is followed by the expressions of the helicity amplitudes, angular coefficients and the physical observables for the decay  $B_c \rightarrow D_s^*(\rightarrow D_s\gamma, D_s\pi)\mu^+\mu^-$ . In section 3, we present the phenomenological analysis of all the observables, in the SM and the NP scenarios, and section 4 concludes our discussion.

## 2 Theoretical Framework

In this section, we present the effective Hamiltonian which is used to compute the full angular distribution of  $B_c \rightarrow D_s^* \rightarrow (D_s \gamma, D_s \pi) \mu^+ \mu^-$  decays. We give the expressions of the helicity amplitudes and express all the angular coefficients in terms these helicity amplitudes. Using the full form of the four fold angular decay distribution, we can extract the  $q^2$  dependent angular coefficients, which will be used to analyze the effects of various 1D and 2D NP scenarios.

### 2.1 Effective Hamiltonian and Decay Amplitude of $B_c \rightarrow D_s^* \mu^+ \mu^-$

The most general low energy effective Hamiltonian for rare  $|\Delta B| = |\Delta S| = 1$  transition, in the presence of new vector and axial vector operators is written as [48],

$$\mathcal{H}_{\text{eff}} = -\frac{4G_F}{\sqrt{2}} V_{tb} V_{ts}^* \left[ C_7^{\text{eff}} O_7 + C_{7'} O_{7'} + \sum_{i=9,10} \left( (C_i + C_{i\ell}^{\text{NP}}) O_i + C_{i\ell}^{\text{NP}} O_{i'} \right) \right], \quad (1)$$

where  $G_F$  is the Fermi coupling constant,  $V_{ij}$  are the CKM matrix elements. The expressions of the dipole operators  $O_{7(\prime)}$ , and the semileptonic operators  $O_{9(\prime),10(\prime)}$  are given as,

$$\begin{aligned} O_7 &= \frac{e}{16\pi^2} m_b (\bar{s} \sigma_{\mu\nu} P_R b) F^{\mu\nu}, & O_{7'} &= \frac{e}{16\pi^2} m_b (\bar{s} \sigma_{\mu\nu} P_L b) F^{\mu\nu}, \\ O_9 &= \frac{e^2}{16\pi^2} (\bar{s} \gamma_\mu P_L b) (\bar{l} \gamma^\mu l), & O_{9'} &= \frac{e^2}{16\pi^2} (\bar{s} \gamma_\mu P_R b) (\bar{l} \gamma^\mu l), \\ O_{10} &= \frac{e^2}{16\pi^2} (\bar{s} \gamma_\mu P_L b) (\bar{l} \gamma^\mu \gamma_5 l), & O_{10'} &= \frac{e^2}{16\pi^2} (\bar{s} \gamma_\mu P_R b) (\bar{l} \gamma^\mu \gamma_5 l), \end{aligned} \quad (2)$$

where  $e$  ( $g_s$ ) is the electromagnetic (strong) coupling constant, and  $m_b$  in  $O_{7(\prime)}$ , is assumed to be the running  $b$ -quark mass in the  $\overline{\text{MS}}$  scheme.  $O_{i'}$  are the chirality flipped operators. Within the SM, contributions of  $O_{7'}$  operator are suppressed by  $m_s/m_b$ , therefore we neglect them and further we do not consider NP scenarios with radiative coefficients  $C_{7(\prime)}^{\text{NP}}$  as they are well constrained [50]. Moreover, for the present study, we have ignored the non-factorizable contributions such as the long distance charm-loop corrections in the effective Hamiltonian, although they are expected to be significant at large recoil.

In Eq.(1),  $C_i(\mu)$  are the corresponding Wilson coefficients at the energy scale  $\mu$ . The expressions of the  $C_7^{\text{eff}}(q^2)$  and  $C_9^{\text{eff}}(q^2)$  Wilson coefficients [51–56], that contain the factorizable contributions from current-current, QCD penguins and chromomagnetic dipole operators  $O_{1-6,8}$  are explicitly given in appendix A. Using the above effective Hamiltonian, the amplitude for the  $B_c \rightarrow D_s^* \ell^+ \ell^-$  decay in the framework of SM as well as NP can be written as,

$$\mathcal{M}(B_c \rightarrow D_s^* \ell^+ \ell^-) = \frac{G_F \alpha}{2\sqrt{2}\pi} V_{tb} V_{ts}^* \left\{ T_\mu^{1,D_s^*} (\bar{\ell} \gamma^\mu \ell) + T_\mu^{2,D_s^*} (\bar{\ell} \gamma^\mu \gamma_5 \ell) \right\}, \quad (3)$$

where

$$\begin{aligned} T_\mu^{1,D_s^*} &= (C_9^{\text{eff}} + C_{9\ell}^{\text{NP}}) \left\langle D_s^*(k, \varepsilon) | \bar{s} \gamma_\mu (1 - \gamma_5) b | B_c(p) \right\rangle + C_{9'\ell}^{\text{NP}} \left\langle D_s^*(k, \varepsilon) | \bar{s} \gamma_\mu (1 + \gamma_5) b | B_c(p) \right\rangle \\ &\quad - \frac{2m_b}{q^2} C_7^{\text{eff}} \left\langle D_s^*(k, \varepsilon) | \bar{s} i \sigma_{\mu\nu} q^\nu (1 + \gamma_5) b | B_c(p) \right\rangle, \end{aligned} \quad (4)$$

$$T_\mu^{2,D_s^*} = (C_{10} + C_{10\ell}^{\text{NP}}) \left\langle D_s^*(k, \varepsilon) | \bar{s} \gamma_\mu (1 - \gamma_5) b | B_c(p) \right\rangle + C_{10'\ell}^{\text{NP}} \left\langle D_s^*(k, \varepsilon) | \bar{s} \gamma_\mu (1 + \gamma_5) b | B_c(p) \right\rangle. \quad (5)$$

where  $T_\mu^{i,D_s^*}$ ,  $i = (1, 2)$ , contain the matrix elements of  $B_c \rightarrow D_s^*$ .

## 2.2 Matrix Elements for $B_c \rightarrow D_s^* \mu^+ \mu^-$ Decay

The hadronic matrix element for  $B_c \rightarrow D_s^* \mu^+ \mu^-$  can be parameterized in terms of form factors as follows,

$$\langle D_s^*(k, \bar{\epsilon}) | \bar{s} \gamma_\mu b | B_c(p) \rangle = \frac{2\epsilon_{\mu\nu\alpha\beta}}{m_{B_c} + m_{D_s^*}} \bar{\epsilon}^{*\nu} p^\alpha k^\beta V(q^2), \quad (6)$$

$$\begin{aligned} \langle D_s^*(k, \bar{\epsilon}) | \bar{s} \gamma_\mu \gamma_5 b | B_c(p) \rangle &= i (m_{B_c} + m_{D_s^*}) g_{\mu\nu} \bar{\epsilon}^{*\nu} A_1(q^2) \\ &\quad - iP_\mu(\bar{\epsilon}^* \cdot q) \frac{A_2(q^2)}{(m_{B_c} + m_{D_s^*})} \\ &\quad - i \frac{2m_{D_s^*}}{q^2} q_\mu (\bar{\epsilon}^* \cdot q) [A_3(q^2) - A_0(q^2)], \end{aligned} \quad (7)$$

where  $P_\mu = p_\mu + k_\mu$ ,  $q_\mu = p_\mu - k_\mu$ , and

$$A_3(q^2) = \frac{m_{B_c} + m_{D_s^*}}{2m_{D_s^*}} A_1(q^2) - \frac{m_{B_c} - m_{D_s^*}}{2m_{D_s^*}} A_2(q^2), \quad (8)$$

with  $A_3(0) = A_0(0)$ . We have used  $\epsilon_{0123} = +1$  convention throughout the study. The additional tensor form factors are expressed as,

$$\langle D_s^*(k, \bar{\epsilon}) | \bar{s} i \sigma_{\mu\nu} q^\nu b | B_c(p) \rangle = -2\epsilon_{\mu\nu\alpha\beta} \bar{\epsilon}^{*\nu} p^\alpha k^\beta T_1(q^2), \quad (9)$$

$$\begin{aligned} \langle D_s^*(k, \bar{\epsilon}) | \bar{s} i \sigma_{\mu\nu} q^\nu \gamma_5 b | B_c(p) \rangle &= i \left[ (m_{B_c}^2 - m_{D_s^*}^2) g_{\mu\nu} \bar{\epsilon}^{*\nu} \right. \\ &\quad \left. - (\bar{\epsilon}^* \cdot q) P_\mu \right] T_2(q^2) + i(\bar{\epsilon}^* \cdot q) \\ &\quad \times \left[ q_\mu - \frac{q^2}{m_{B_c}^2 - m_{D_s^*}^2} P_\mu \right] T_3(q^2). \end{aligned} \quad (10)$$

## 2.3 Helicity Formalism of $B_c \rightarrow D_s^* \mu^+ \mu^-$ Decay

For  $B_c \rightarrow D_s^* \mu^+ \mu^-$  decay, the amplitude can be expressed in terms of helicity basis. For kinematics of the four-body decay (see Fig. 1), we closely follow Ref. [57], where detailed formalism is given. The completeness and orthogonality properties of helicity basis can be expressed as follows,

$$\varepsilon^{*\alpha}(n) \varepsilon_\alpha(l) = g_{nl}, \quad \sum_{n,l=t,+,-,0} \varepsilon^{*\alpha}(n) \varepsilon^\beta(l) g_{nl} = g^{\alpha\beta}, \quad (11)$$

with  $g_{nl} = \text{diag}(+, -, -, -)$ . From the completeness relation given in Eq. (11), the contraction of leptonic tensors  $L^{(k)\alpha\beta}$  and hadronic tensors  $H_{\alpha\beta}^{ij} = T_\alpha^{i,D_s^*} \bar{T}_\beta^{j,D_s^*}$  ( $i, j = 1, 2$ ), can be written as

$$L^{(k)\alpha\beta} H_{\alpha\beta}^{ij} = \sum_{n,n',l,l'} L_{nl}^{(k)} g_{nn'} g_{ll'} H_{n'l'}^{ij}, \quad (12)$$

where the leptonic and hadronic tensors can be written in the helicity basis as follows

$$L_{nl}^{(k)} = \varepsilon^\alpha(n) \varepsilon^{*\beta}(l) L_{\alpha\beta}^{(k)}, \quad H_{nl}^{ij} = \varepsilon^{*\alpha}(n) \varepsilon^\beta(l) H_{\alpha\beta}^{ij}. \quad (13)$$

Both leptonic and hadronic tensors shown in Eq. (13), can be evaluated in two different frame

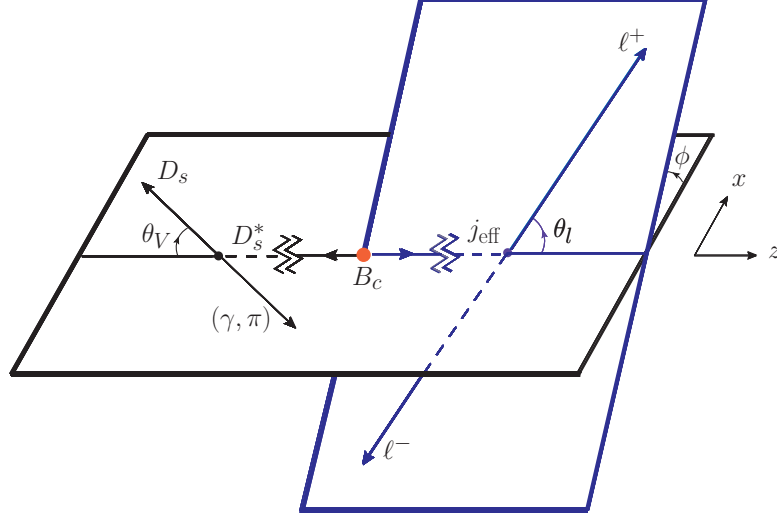


Figure 1: Kinematics of the  $B_c \rightarrow D_s^*(\rightarrow D_s\gamma, (D_s\pi))\ell^+\ell^-$  decays.

of references. The lepton tensor  $L_{nl}^{(k)}$  is evaluated in  $\mu^+\mu^-$  centre of mass (CM) frame, and the hadronic tensor  $H_{nl}^{ij}$  is evaluated in the rest frame of  $B_c$  meson. For the said decay one can write the hadronic tensor as follows,

$$\begin{aligned} H_{nl}^{ij} &= (\varepsilon^{*\alpha}(n)T_\alpha^{i,D_s^*}) \cdot \overline{(\varepsilon^{*\beta}(l)T_\beta^{j,D_s^*})} \\ &= (\varepsilon^{*\alpha}(n)\bar{\varepsilon}^{*\mu}(r)T_{\alpha,\mu}^{i,D_s^*}) \cdot \overline{(\varepsilon^{*\beta}(l)\bar{\varepsilon}^{*\nu}(s)T_{\beta,\nu}^{j,D_s^*})} \delta_{rs} \equiv H_n^{i,D_s^*} \bar{H}_l^{j,D_s^*}, \end{aligned} \quad (14)$$

where, from angular momentum conservation,  $r = n$  and  $s = l$  for  $n, l = \pm, 0$  and  $r, s = 0$  for  $n, l = t$ . The explicit expressions of the helicity amplitudes for  $B_c \rightarrow D_s^*$ , are obtained in terms of the SM and NP Wilson coefficients as,

$$\begin{aligned} H_t^{1,D_s^*} &= -i\sqrt{\frac{\lambda}{q^2}}(C_9^{\text{eff}} + C_{9\ell}^{\text{NP}} - C_{9'\ell}^{\text{NP}})A_0, \\ H_t^{2,D_s^*} &= -i\sqrt{\frac{\lambda}{q^2}}(C_{10} + C_{10\ell}^{\text{NP}} - C_{10'\ell}^{\text{NP}})A_0, \\ H_\pm^{1,D_s^*} &= -i(m_{B_c}^2 - m_{D_s^*}^2) \left[ (C_9^{\text{eff}} + C_{9\ell}^{\text{NP}} - C_{9'\ell}^{\text{NP}}) \frac{A_1}{(m_{B_c} - m_{D_s^*})} \right. \\ &\quad \left. + \frac{2m_b}{q^2} C_7^{\text{eff}} T_2 \right] \pm i\sqrt{\lambda} \left[ (C_9^{\text{eff}} + C_{9\ell}^{\text{NP}} + C_{9'\ell}^{\text{NP}}) \frac{V}{(m_{B_c} + m_{D_s^*})} + \frac{2m_b}{q^2} C_7^{\text{eff}} T_1 \right], \\ H_\pm^{2,D_s^*} &= -i(C_{10} + C_{10\ell}^{\text{NP}} - C_{10'\ell}^{\text{NP}}) (m_{B_c} + m_{D_s^*}) A_1 \\ &\quad \pm i\sqrt{\lambda} (C_{10} + C_{10\ell}^{\text{NP}} + C_{10'\ell}^{\text{NP}}) \frac{V}{(m_{B_c} + m_{D_s^*})}, \\ H_0^{1,D_s^*} &= -\frac{i}{2m_{D_s^*}\sqrt{q^2}} \left[ (C_9^{\text{eff}} + C_{9\ell}^{\text{NP}} - C_{9'\ell}^{\text{NP}}) \left\{ (m_{B_c}^2 - m_{D_s^*}^2 - q^2) (m_{B_c} + m_{D_s^*}) A_1 \right. \right. \\ &\quad \left. \left. - \frac{\lambda}{m_{B_c} + m_{D_s^*}} A_2 \right\} + 2m_b C_7^{\text{eff}} \left\{ (m_{B_c}^2 + 3m_{D_s^*}^2 - q^2) T_2 - \frac{\lambda}{m_{B_c}^2 - m_{D_s^*}^2} T_3 \right\} \right], \end{aligned}$$

$$H_0^{2,D_s^*} = -\frac{i}{2m_{D_s^*}\sqrt{q^2}}(C_{10} + C_{10\ell}^{\text{NP}} - C_{10\ell}^{\text{NP}}) \left[ (m_{B_c}^2 - m_{D_s^*}^2 - q^2)(m_{B_c} + m_{D_s^*}) A_1 - \frac{\lambda}{m_{B_c} + m_{D_s^*}} A_2 \right]. \quad (15)$$

## 2.4 Four-fold Angular Distribution of $B_c \rightarrow D_s^*(\rightarrow D_s\gamma(D_s\pi))\ell^+\ell^-$ Decays

In an effective theory, the NP effects are due to the Wilson coefficients and new operators given in Eq. (1). For the decay modes  $B_c \rightarrow D_s^*(\rightarrow D_s\gamma(D_s\pi))\ell^+\ell^-$ , these effects are contained in the four-dimensional differential decay distribution that depends on the square of the momentum transfer  $q^2$ , angles  $\theta_\ell$ ,  $\theta_V$ , and  $\phi$  as described in Fig. 1. For the decays under consideration, the full differential angular distribution can be written as,

$$\begin{aligned} \frac{d^4\Gamma(B_c \rightarrow D_s^*(\rightarrow D_s\gamma(D_s\pi))\ell^+\ell^-)}{dq^2 d\cos\theta_\ell d\cos\theta_V d\phi} &= \frac{9}{32\pi} \mathcal{B}(D_s^* \rightarrow D_s\gamma(D_s\pi)) \\ &\times \left[ I_{1s,\perp}^\gamma(I_{1s,\parallel}) \sin^2\theta_V + I_{1c,\perp}^\gamma(I_{1c,\parallel}) \cos^2\theta_V \right. \\ &+ \left( I_{2s,\perp}^\gamma(I_{2s,\parallel}) \sin^2\theta_V + I_{2c,\perp}^\gamma(I_{2c,\parallel}) \cos^2\theta_V \right) \cos 2\theta_\ell \\ &+ \left( I_{6s,\perp}^\gamma(I_{6s,\parallel}) \sin^2\theta_V + I_{6c,\perp}^\gamma \cos^2\theta_V \right) \cos\theta_\ell \\ &+ \left( I_{3,\perp}^\gamma(I_{3,\parallel}) \cos 2\phi + I_{9,\perp}^\gamma(I_{9,\parallel}) \sin 2\phi \right) \sin^2\theta_V \sin^2\theta_\ell \\ &+ \left( I_{4,\perp}^\gamma(I_{4,\parallel}) \cos\phi + I_{8,\perp}^\gamma(I_{8,\parallel}) \sin\phi \right) \sin 2\theta_V \sin 2\theta_\ell \\ &+ \left. \left( I_{5,\perp}^\gamma(I_{5,\parallel}) \cos\phi + I_{7,\perp}^\gamma(I_{7,\parallel}) \sin\phi \right) \sin 2\theta_V \sin\theta_\ell \right], \quad (16) \end{aligned}$$

where  $I_{n\lambda,\perp}^\gamma$  and  $I_{n\lambda,\parallel}$  are the angular coefficients. The explicit expressions of  $I_{n\lambda,\perp}^\gamma$  in terms of the helicity amplitudes are obtained as,

$$\begin{aligned} I_{1s,\perp}^\gamma &= \frac{(2 + \beta_l^2)}{4} N^2 (|H_+^1|^2 + |H_+^2|^2 + |H_-^1|^2 + |H_-^2|^2) + (|H_0^1|^2 + |H_0^2|^2) \\ &+ \frac{2m_l^2}{q^2} N^2 \left[ (|H_+^1|^2 - |H_+^2|^2 + |H_-^1|^2 - |H_-^2|^2) + 2(|H_0^1|^2 - |H_0^2|^2 + 2|H_t^2|^2) \right], \quad (17) \end{aligned}$$

$$\begin{aligned} I_{1c,\perp}^\gamma &= \frac{(2 + \beta_l^2)}{2} N^2 (|H_+^1|^2 + |H_+^2|^2 + |H_-^1|^2 + |H_-^2|^2) \\ &+ \frac{4m_l^2}{q^2} N^2 (|H_+^1|^2 - |H_+^2|^2 + |H_-^1|^2 - |H_-^2|^2), \quad (18) \end{aligned}$$

$$I_{2s,\perp}^\gamma = -\beta_l^2 N^2 \left[ (|H_0^1|^2 + |H_0^2|^2) - \frac{1}{4} (|H_+^1|^2 + |H_+^2|^2 + |H_-^1|^2 + |H_-^2|^2) \right], \quad (19)$$

$$I_{2c,\perp}^\gamma = \frac{\beta_l^2}{2} N^2 (|H_+^1|^2 + |H_+^2|^2 + |H_-^1|^2 + |H_-^2|^2), \quad (20)$$

$$I_{3,\perp}^\gamma = \beta_l^2 N^2 \left[ \mathcal{R}e(H_+^1 H_-^{1*} + H_+^2 H_-^{2*}) \right], \quad (21)$$

$$I_{4,\perp}^\gamma = -\frac{\beta_l^2}{2} N^2 \left[ \mathcal{R}e(H_+^1 H_0^{1*} + H_-^1 H_0^{1*}) + \mathcal{R}e(H_+^2 H_0^{2*} + H_-^2 H_0^{2*}) \right], \quad (22)$$

$$I_{5,\perp}^\gamma = \beta_l N^2 \left[ \mathcal{R}e (H_+^1 H_0^{2*} - H_-^1 H_0^{2*}) + \mathcal{R}e (H_+^2 H_0^{1*} - H_-^2 H_0^{1*}) \right], \quad (23)$$

$$I_{6s,\perp}^\gamma = -2\beta_l N^2 \left[ \mathcal{R}e (H_+^1 H_+^{2*} - H_-^1 H_-^{2*}) \right], \quad (24)$$

$$I_{6c,\perp}^\gamma = -4\beta_l N^2 \left[ \mathcal{R}e (H_+^1 H_+^{2*} - H_-^1 H_-^{2*}) \right], \quad (25)$$

$$I_{7,\perp}^\gamma = \beta_l N^2 \left[ \mathcal{I}m (H_0^1 H_+^{2*} + H_0^1 H_-^{2*}) + \mathcal{I}m (H_0^2 H_+^{1*} + H_0^2 H_-^{1*}) \right], \quad (26)$$

$$I_{8,\perp}^\gamma = -\frac{\beta_l^2}{2} N^2 \left[ \mathcal{I}m (H_0^1 H_+^{1*} - H_0^1 H_-^{1*}) + \mathcal{I}m (H_0^2 H_+^{2*} - H_0^2 H_-^{2*}) \right], \quad (27)$$

$$I_{9,\perp}^\gamma = -\beta_l^2 N^2 \left[ \mathcal{I}m (H_+^1 H_-^{1*} + H_+^2 H_-^{2*}) \right], \quad (28)$$

whereas the expressions of  $I_{n\lambda,\parallel}$  in terms of the helicity amplitudes are written as,

$$I_{1s,\parallel} = \frac{(2 + \beta_l^2)}{2} N^2 (|H_+^1|^2 + |H_+^2|^2 + |H_-^1|^2 + |H_-^2|^2) + \frac{4m_l^2}{q^2} N^2 (|H_+^1|^2 - |H_+^2|^2 + |H_-^1|^2 - |H_-^2|^2), \quad (29)$$

$$I_{1c,\parallel} = 2N^2 (|H_0^1|^2 + |H_0^2|^2) + \frac{8m_l^2}{q^2} N^2 (|H_0^1|^2 - |H_0^2|^2 + 2|H_t^2|^2), \quad (30)$$

$$I_{2s,\parallel} = \frac{\beta_l^2}{2} N^2 (|H_+^1|^2 + |H_+^2|^2 + |H_-^1|^2 + |H_-^2|^2), \quad (31)$$

$$I_{2c,\parallel} = -2\beta_l^2 N^2 (|H_0^1|^2 + |H_0^2|^2), \quad (32)$$

$$I_{3,\parallel} = -2\beta_l^2 N^2 \left[ \mathcal{R}e (H_+^1 H_-^{1*} + H_+^2 H_-^{2*}) \right], \quad (33)$$

$$I_{4,\parallel} = \beta_l^2 N^2 \left[ \mathcal{R}e (H_+^1 H_0^{1*} + H_-^1 H_0^{1*}) + \mathcal{R}e (H_+^2 H_0^{2*} + H_-^2 H_0^{2*}) \right], \quad (34)$$

$$I_{5,\parallel} = -2\beta_l N^2 \left[ \mathcal{R}e (H_+^1 H_0^{2*} - H_-^1 H_0^{2*}) + \mathcal{R}e (H_+^2 H_0^{1*} - H_-^2 H_0^{1*}) \right], \quad (35)$$

$$I_{6s,\parallel} = -4\beta_l N^2 \left[ \mathcal{R}e (H_+^1 H_+^{2*} - H_-^1 H_-^{2*}) \right], \quad (36)$$

$$I_{6c,\parallel} = 0, \quad (37)$$

$$I_{7,\parallel} = -2\beta_l N^2 \left[ \mathcal{I}m (H_0^1 H_+^{2*} + H_0^1 H_-^{2*}) + \mathcal{I}m (H_0^2 H_+^{1*} + H_0^2 H_-^{1*}) \right], \quad (38)$$

$$I_{8,\parallel} = \beta_l^2 N^2 \left[ \mathcal{I}m (H_0^1 H_+^{1*} - H_0^1 H_-^{1*}) + \mathcal{I}m (H_0^2 H_+^{2*} - H_0^2 H_-^{2*}) \right], \quad (39)$$

$$I_{9,\parallel} = 2\beta_l^2 N^2 \left[ \mathcal{I}m (H_+^1 H_-^{1*} + H_+^2 H_-^{2*}) \right], \quad (40)$$

where

$$N = V_{tb} V_{ts}^* \left[ \frac{G_F^2 \alpha^2}{3.2^{10} \pi^5 m_{B_c}^3} q^2 \sqrt{\lambda} \beta_l \right]^{1/2}, \quad (41)$$

with  $\lambda \equiv \lambda(m_{B_c}^2, m_{D_s^*}^2, q^2)$  and  $\beta_l = \sqrt{1 - 4m_l^2/q^2}$ .

## 2.5 Physical Observables for $B_c \rightarrow D_s^*(\rightarrow D_s\gamma(D_s\pi))\ell^+\ell^-$ Decays

In this section, we construct the physical observables for the  $B_c \rightarrow D_s^*(\rightarrow D_s\gamma(D_s\pi))\ell^+\ell^-$  decays, in terms of the angular coefficients. The observables which we consider are the differential branching ratios ( $d\mathcal{B}/dq^2$ ), lepton forward-backward asymmetry ( $A_{\text{FB}}$ ), longitudinal polarization fraction of  $D_s^*$  ( $f_L$ ), unpolarized ( $R_{D_s^*}$ ), and polarized ( $R_{D_s^*}^{L,T}$ ) LFUV ratios, and the angular coefficients ( $\langle I_{n\lambda,\perp}^\gamma \rangle, \langle I_{n\lambda,\parallel} \rangle$ ). Other than the differential decay rates and the ratios, all observables are normalized to the corresponding differential decay rate.

**(i) Differential decay rates:** From the full angular distribution Eq. (16),  $q^2$  dependent differential decay rate expressions are obtained in terms of angular coefficients as follows,

$$\begin{aligned} \frac{d\Gamma(B_c \rightarrow D_s^*\mu^+\mu^-)}{dq^2} &= \frac{1}{4}(3I_{1c,\perp}^\gamma + 6I_{1s,\perp}^\gamma - I_{2c,\perp}^\gamma - 2I_{2s,\perp}^\gamma) \\ &= \frac{1}{4}(3I_{1c,\parallel} + 6I_{1s,\parallel} - I_{2c,\parallel} - 2I_{2s,\parallel}). \end{aligned} \quad (42)$$

$$\frac{d\Gamma(B_c \rightarrow D_s^*(\rightarrow D_s\gamma)\mu^+\mu^-)}{dq^2} = \mathcal{B}(D_s^* \rightarrow D_s\gamma) \frac{1}{4}(3I_{1c,\perp}^\gamma + 6I_{1s,\perp}^\gamma - I_{2c,\perp}^\gamma - 2I_{2s,\perp}^\gamma). \quad (43)$$

$$\frac{d\Gamma(B_c \rightarrow D_s^*(\rightarrow D_s\pi)\mu^+\mu^-)}{dq^2} = \mathcal{B}(D_s^* \rightarrow D_s\pi) \frac{1}{4}(3I_{1c,\parallel} + 6I_{1s,\parallel} - I_{2c,\parallel} - 2I_{2s,\parallel}). \quad (44)$$

**(ii) Lepton forward backward asymmetry:** The lepton forward backward asymmetry as a function of  $q^2$  can be expressed as,

$$A_{\text{FB}}(q^2) = \frac{3(I_{6c,\perp}^\gamma + 2I_{6s,\perp}^\gamma)}{2(3I_{1c,\perp}^\gamma + 6I_{1s,\perp}^\gamma - I_{2c,\perp}^\gamma - 2I_{2s,\perp}^\gamma)} = \frac{6I_{6s,\parallel}}{2(3I_{1c,\parallel} + 6I_{1s,\parallel} - I_{2c,\parallel} - 2I_{2s,\parallel})}. \quad (45)$$

**(iii) Longitudinal helicity fraction:** The longitudinal helicity fraction of the decay  $B_c \rightarrow D_s^*(\rightarrow D_s\gamma, (D_s\pi))\mu^+\mu^-$ , when  $D_s^*$  meson is longitudinally polarized can be expressed as,

$$f_L(q^2) = \frac{(6I_{1s,\perp}^\gamma - 2I_{2s,\perp}^\gamma) - (3I_{1c,\perp}^\gamma - I_{2c,\perp}^\gamma)}{3I_{1c,\perp}^\gamma + 6I_{1s,\perp}^\gamma - I_{2c,\perp}^\gamma - 2I_{2s,\perp}^\gamma} = \frac{3I_{1c,\parallel} - I_{2c,\parallel}}{3I_{1c,\parallel} + 6I_{1s,\parallel} - I_{2c,\parallel} - 2I_{2s,\parallel}}. \quad (46)$$

**(iv) LFUV ratios for  $B_c \rightarrow D_s^*\ell^+\ell^-$  Decay:** The unpolarized and polarized LFUV for the decay  $B_c \rightarrow D_s^*\ell^+\ell^-$  can be written as,

$$R_{D_s^*}[q_{\min}^2, q_{\max}^2] = \frac{\int_{q_{\min}^2}^{q_{\max}^2} (d\mathcal{B}(B_c \rightarrow D_s^*\mu^+\mu^-)/dq^2) dq^2}{\int_{q_{\min}^2}^{q_{\max}^2} (d\mathcal{B}(B_c \rightarrow D_s^*e^+e^-)/dq^2) dq^2}, \quad (47)$$

$$R_{D_s^*}^{L,T}[q_{\min}^2, q_{\max}^2] = \frac{\int_{q_{\min}^2}^{q_{\max}^2} (d\mathcal{B}(B_c \rightarrow D_s^{*L,T}\mu^+\mu^-)/dq^2) dq^2}{\int_{q_{\min}^2}^{q_{\max}^2} (d\mathcal{B}(B_c \rightarrow D_s^{*L,T}e^+e^-)/dq^2) dq^2}. \quad (48)$$

**(v) Normalized angular observables:**

$$\langle I_{n\lambda,\parallel} \rangle = \frac{I_{n\lambda,\parallel}}{d\Gamma/dq^2}, \quad \langle I_{n\lambda,\perp}^\gamma \rangle = \frac{I_{n\lambda,\perp}^\gamma}{d\Gamma/dq^2}. \quad (49)$$

**(vi) Binned normalized angular observables:**

$$\langle I_{n\lambda,\parallel} \rangle [q_{\min}^2, q_{\max}^2] = \frac{\int_{q_{\min}^2}^{q_{\max}^2} I_{n\lambda,\parallel} dq^2}{\int_{q_{\min}^2}^{q_{\max}^2} (d\Gamma/dq^2) dq^2}, \quad \langle I_{n\lambda,\perp}^\gamma \rangle [q_{\min}^2, q_{\max}^2] = \frac{\int_{q_{\min}^2}^{q_{\max}^2} I_{n\lambda,\perp}^\gamma dq^2}{\int_{q_{\min}^2}^{q_{\max}^2} (d\Gamma/dq^2) dq^2}. \quad (50)$$



### 3 Phenomenological Analysis

#### 3.1 Input Parameters

To investigate NP effects in the observables of the  $B_c \rightarrow D_s^*(\rightarrow D_s\gamma, (D_s\pi))\ell^+\ell^-$  decays, we use input parameters such as the transition form factors, which are calculated in the framework of the relativistic quark model (RQM) [58]. The RQM, based on the quasipotential approach, reliably determines the form factors in the whole  $q^2$  range by incorporating relativistic effects including contributions of intermediate negative energy states and relativistic transformations of the meson wave functions. Furthermore, the form factors obtained in the RQM, satisfy all the model independent symmetry relations arising in the limits of heavy quark mass and large recoil of the final meson [59]. The form factors calculated, in the RQM, through the overlap integrals of the initial and final meson relativistic wave functions [58], can be expressed in terms of the expressions involving fitted parameters. Such as, the form factors,  $V(q^2)$ ,  $A_0(q^2)$  and  $T_1(q^2)$  given in Eqs. (6, 7), and (9), are parameterized in the whole kinematical  $q^2$  region as,

$$F(q^2) = \frac{F(0)}{\left(1 - \frac{q^2}{M^2}\right)\left(1 - \sigma_1 \frac{q^2}{M_{B_s^*}^2} + \sigma_2 \frac{q^4}{M_{B_s^*}^4}\right)}, \quad (51)$$

where the form factor  $A_0(q^2)$  contains a pole at  $q^2 = M^2 \equiv M_{B_s^*}^2$  and the form factors  $V(q^2)$ ,  $T_1(q^2)$  contain pole at  $q^2 = M^2 \equiv M_{B_s^*}^2$ . The numerical values of these pole masses are  $M_{B_s} = 5.36692$  GeV, and  $M_{B_s^*} = 5.4154$  GeV [60]. Moreover, the form factors  $A_1(q^2)$ ,  $A_2(q^2)$ ,  $T_2(q^2)$ , and  $T_3(q^2)$ , given in Eq. (7), and Eq. (10), can be parameterized as follows,

$$F(q^2) = \frac{F(0)}{\left(1 - \sigma_1 \frac{q^2}{M_{B_s^*}^2} + \sigma_2 \frac{q^4}{M_{B_s^*}^4}\right)}. \quad (52)$$

For completeness, the numerical values of form factors at  $q^2 = 0$ , and fitted parameters  $\sigma_1$  and  $\sigma_2$ , are collected in Table 1. In order to gauge the effects of the form factor uncertainties on various observables, we allow the parameters in the fitted form factors to deviate by  $\pm 5\%$ . The numerical values of Wilson coefficients in the SM, evaluated at the renormalization scale

Table 1: The numerical values of transition form factors for  $B_c \rightarrow D_s^*\mu^+\mu^-$  decay at  $q^2 = 0$ , and the fitted parameters  $\sigma_1$  and  $\sigma_2$  [58]. The reported uncertainties represent the  $\pm 5\%$  deviations in the parameters of the fitted form factors.

	$V$	$A_0$	$A_1$	$A_2$	$T_1$	$T_2$	$T_3$
$F(0)$	$0.182_{-0.010}^{+0.010}$	$0.070_{-0.004}^{+0.004}$	$0.089_{-0.005}^{+0.005}$	$0.110_{-0.006}^{+0.006}$	$0.085_{-0.005}^{+0.005}$	$0.085_{-0.004}^{+0.004}$	$0.051_{-0.003}^{+0.003}$
$\sigma_1$	$2.133_{-0.107}^{+0.107}$	$1.561_{-0.078}^{+0.078}$	$2.479_{-0.124}^{+0.124}$	$2.833_{-0.142}^{+0.142}$	$1.540_{-0.077}^{+0.077}$	$2.577_{-0.129}^{+0.129}$	$2.783_{-0.139}^{+0.139}$
$\sigma_2$	$1.183_{-0.059}^{+0.059}$	$0.192_{-0.010}^{+0.010}$	$1.686_{-0.084}^{+0.084}$	$2.167_{-0.108}^{+0.108}$	$0.248_{-0.013}^{+0.013}$	$1.859_{-0.093}^{+0.093}$	$2.170_{-0.109}^{+0.109}$

$\mu \sim m_b$  [61], are presented in Table 2. The other input parameters are listed in Table 3.

Table 2: The numerical values of the SM Wilson coefficients up to NNLL accuracy, evaluated at the renormalization scale  $\mu \sim m_b$  [61].

$C_1$	$C_2$	$C_3$	$C_4$	$C_5$	$C_6$	$C_7$	$C_8$	$C_9$	$C_{10}$
-0.294	1.017	-0.0059	-0.087	0.0004	0.0011	-0.324	-0.176	4.114	-4.193

Table 3: Values of different input parameters used in the numerical analysis.

$M_{B_c} = 6.27 \text{ GeV}, m_b = 4.28 \text{ GeV}, m_s = 0.13 \text{ GeV},$ $m_\mu = 0.105 \text{ GeV}, m_\tau = 1.77 \text{ GeV},$ $\mathcal{B}(D_s^* \rightarrow D_s \gamma) = 93.5 \times 10^{-2}, \mathcal{B}(D_s^* \rightarrow D_s \pi) = 5.8 \times 10^{-2}$ $ V_{tb}V_{ts}^*  = 45 \times 10^{-3}, \alpha^{-1} = 137, G_F = 1.17 \times 10^{-5} \text{ GeV}^{-2},$ $\tau_{B_c} = 0.46 \times 10^{-12} \text{ sec}, M_{D_s^*} = 2.1123 \text{ GeV}.$
--

### 3.2 NP Scenarios

In this section, we first specify our choice of the NP scenarios which are used to investigate the effects of NP on various physical observables in the angular distribution of  $B_c \rightarrow D_s^*(\rightarrow D_s \gamma)\mu^+\mu^-$  and  $B_c \rightarrow D_s^*(\rightarrow D_s \pi)\mu^+\mu^-$  decays in a model independent framework. We choose the best fit values of NP couplings in different scenarios, from the recent global fit analysis [42]. The global fit analysis performed by authors of Ref. [42], shows that with the assumption of NP present only in the muon sector, two 1D NP scenarios  $C_{9\mu}^{\text{NP}} < 0$ , and  $C_{9\mu}^{\text{NP}} = -C_{10\mu}^{\text{NP}}$ , continue to be the most favored scenarios, whereas the 2D scenarios  $(C_{9\mu}^{\text{NP}}, C_{10'\mu}^{\text{NP}})$ ,  $(C_{9\mu}^{\text{NP}}, C_{9'\mu}^{\text{NP}})$  and  $(C_{9\mu}^{\text{NP}}, C_{10\mu}^{\text{NP}})$  provide better fit to data with preference decreasing in the listed order. The best fit values of these 1D and 2D NP scenarios are listed in Table-4.

Table 4: Best-fit values of the 1D and 2D NP scenarios considering NP in muon sector only [42].

Scenario		Best-fit value
S1	$C_{9\mu}^{\text{NP}}$	-0.98
S2	$C_{9\mu}^{\text{NP}} = -C_{10\mu}^{\text{NP}}$	-0.46
S3	$(C_{9\mu}^{\text{NP}}, C_{10'\mu}^{\text{NP}})$	(-1.15, -0.26)
S4	$(C_{9\mu}^{\text{NP}}, C_{9'\mu}^{\text{NP}})$	(-1.12, 0.40)
S5	$(C_{9\mu}^{\text{NP}}, C_{10\mu}^{\text{NP}})$	(-0.80, 0.24)

### 3.3 Analysis of Physical Observables in $B_c \rightarrow D_s^*(\rightarrow D_s \gamma, (D_s \pi))\ell^+\ell^-$ Decays

In this section, we now analyze the NP effects via observables which are constructed from the combination of the angular coefficients, such as the differential branching ratios ( $d\mathcal{B}/dq^2$ ), lepton forward-backward asymmetry ( $A_{\text{FB}}$ ), longitudinal polarization fraction of  $D_s^*$  ( $f_L$ ), unpolarized ( $R_{D_s^*}$ ), and polarized ( $R_{D_s^*}^{L,T}$ ) LFUV ratios, in  $B_c \rightarrow D_s^*(\rightarrow D_s \gamma, (D_s \pi))\ell^+\ell^-$  decays. Binned averaged numerical values of the SM and NP predictions of all these observables, with errors due to the form factors, in different  $q^2$  bins, are given in Tables 5-11, of appendix B. In Figs. 2-3, we plot differential branching ratios, forward-backward asymmetry, and the longitudinal polarization fraction of  $D_s^*$ , as a function of  $q^2$ , leading to following observations. Moreover, our results regarding to LFUV ratios, in all NP scenarios, do not show sizable deviations from the SM predictions, therefore, we do not present their  $q^2$  plots.

- In Fig. 2(a) and 2(b), we have plotted the differential branching ratios for  $B_c \rightarrow D_s^*(\rightarrow D_s \gamma)\mu^+\mu^-$  and  $B_c \rightarrow D_s^*(\rightarrow D_s \pi)\mu^+\mu^-$  decays as a function of  $q^2$  in the framework of the SM as well as the NP scenarios under consideration. In SM, the differential branching ratio

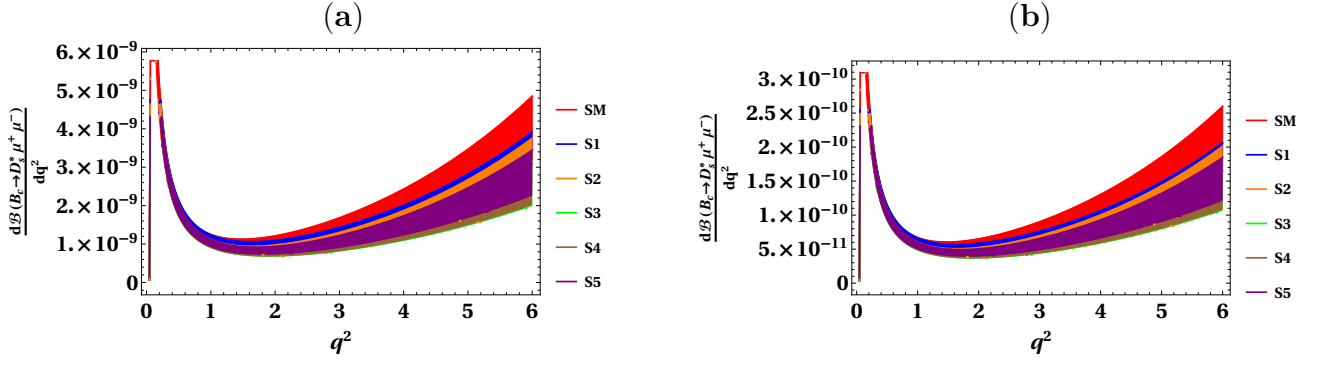


Figure 2: Differential branching ratio for the decay  $B_c \rightarrow D_s^* \mu^+ \mu^-$  in the SM and the NP scenarios. (a) depicts the differential branching ratio for the cascade decay  $B_c \rightarrow D_s^*(\rightarrow D_s \gamma) \mu^+ \mu^-$ , and (b) depicts the differential branching ratio for the cascade decay  $B_c \rightarrow D_s^*(\rightarrow D_s \pi) \mu^+ \mu^-$ .

for  $B_c \rightarrow D_s^*(\rightarrow D_s \gamma) \mu^+ \mu^-$  decay is of the order  $10^{-9}$ , whereas for  $B_c \rightarrow D_s^*(\rightarrow D_s \pi) \mu^+ \mu^-$  decay, it is of the order  $10^{-10}$ . Both Fig. 2(a) and 2(b), depict that NP scenarios predictions are compatible with the SM predictions as the error bands emerging due to the uncertainties of the form factors overlap. However, the central value predictions of all the NP scenarios show trend towards the lesser values of differential branching ratios as compared to the SM expectations.

- Fig. 3, depicts the forward-backward asymmetry ( $A_{FB}$ ), and longitudinal helicity fraction ( $f_L$ ), of  $B_c \rightarrow D_s^* \mu^+ \mu^-$  decay as a function of  $q^2$ , in the SM framework as well as NP scenarios presented in Table 4. Regarding the zero position of the  $A_{FB}$ , it is important to mention here that the uncertainty due to the form factors is small and hence the  $A_{FB}$  provides stringent tests to see the NP effects. Fig. 3(a) shows that the zero position of  $A_{FB}$  shifts towards right for all the NP scenarios. The zero crossing in the  $A_{FB}$  at  $q^2 = 3$   $\text{GeV}^2$ ,  $q^2 = 2.8$   $\text{GeV}^2$ , and  $q^2 = 3.4$   $\text{GeV}^2$  in the presence of NP scenarios (S1, S5), S2, (S3, S4), respectively is quite distinct from the SM prediction at  $q^2 = 2.6$   $\text{GeV}^2$ .
- Another physical observable useful to investigate the structure of NP is the longitudinal helicity fraction of the final state meson ( $f_L$ ). In Fig. 3(b), we have shown the longitudinal

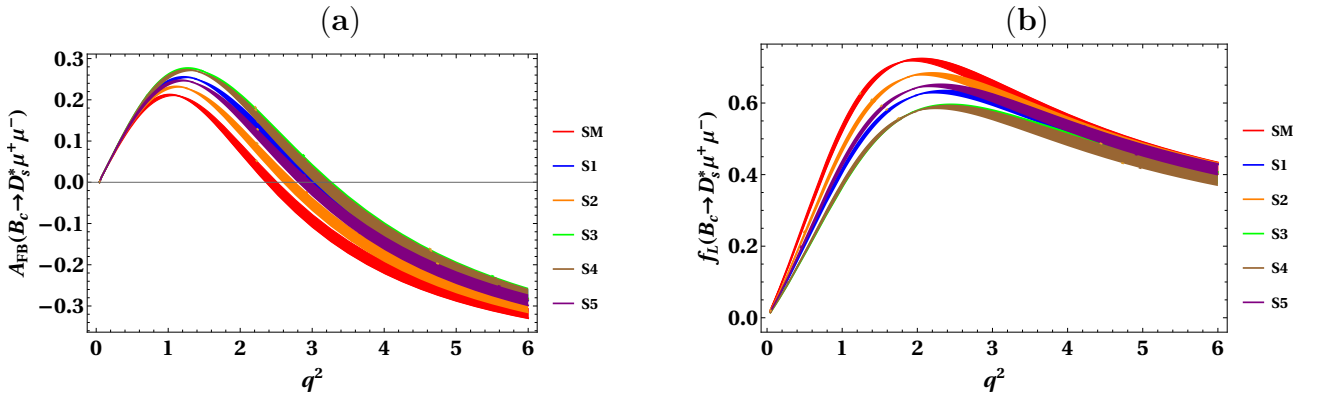


Figure 3: (a) Lepton forward backward asymmetry  $A_{FB}$ , and (b) longitudinal polarization fraction of  $D_s^*$  meson  $f_L$ , for the  $B_c \rightarrow D_s^* \mu^+ \mu^-$  decay, in the SM and the NP scenarios.

helicity fraction  $f_L$  for  $B_c \rightarrow D_s^* \mu^+ \mu^-$  decay as a function of  $q^2$ . We can recognize from Fig. 3(b), that the given NP scenarios in the longitudinal helicity fraction of  $D_s^*$  can be distinguished quite easily in the region  $q^2 = (1 - 2.5)$  GeV<sup>2</sup>, and all the NP predictions point out lesser values of  $f_L$ , compare to the SM. However, for  $q^2 > 2.5$  GeV<sup>2</sup> the given NP scenarios overlap with each other.

### 3.4 Analysis of Angular Coefficients in $B_c \rightarrow D_s^*(\rightarrow D_s \gamma, (D_s \pi)) \mu^+ \mu^-$ Decays

In this section, we analyze the effects of NP via individual angular coefficients such as  $\langle I_{1s,\perp}^\gamma \rangle (\langle I_{1s,\parallel} \rangle)$ ,  $\langle I_{1c,\perp}^\gamma \rangle (\langle I_{1c,\parallel} \rangle)$ ,  $\langle I_{2s,\perp}^\gamma \rangle (\langle I_{2s,\parallel} \rangle)$ ,  $\langle I_{2c,\perp}^\gamma \rangle (\langle I_{2c,\parallel} \rangle)$ ,  $\langle I_{3,\perp}^\gamma \rangle (\langle I_{3,\parallel} \rangle)$ ,  $\langle I_{4,\perp}^\gamma \rangle (\langle I_{4,\parallel} \rangle)$ ,  $\langle I_{5,\perp}^\gamma \rangle (\langle I_{5,\parallel} \rangle)$ ,  $\langle I_{6s,\perp}^\gamma \rangle (\langle I_{6s,\parallel} \rangle)$ , and  $\langle I_{6c,\perp}^\gamma \rangle (\langle I_{6c,\parallel} \rangle)$ , for  $B_c \rightarrow D_s^*(\rightarrow D_s \gamma, (D_s \pi)) \mu^+ \mu^-$  decays. Using the input parameters given in Table 3, we estimate the above mentioned angular observables for both  $B_c \rightarrow D_s^*(\rightarrow D_s \gamma) \mu^+ \mu^-$  and  $B_c \rightarrow D_s^*(\rightarrow D_s \pi) \mu^+ \mu^-$  decays in the SM as well as in 1D and

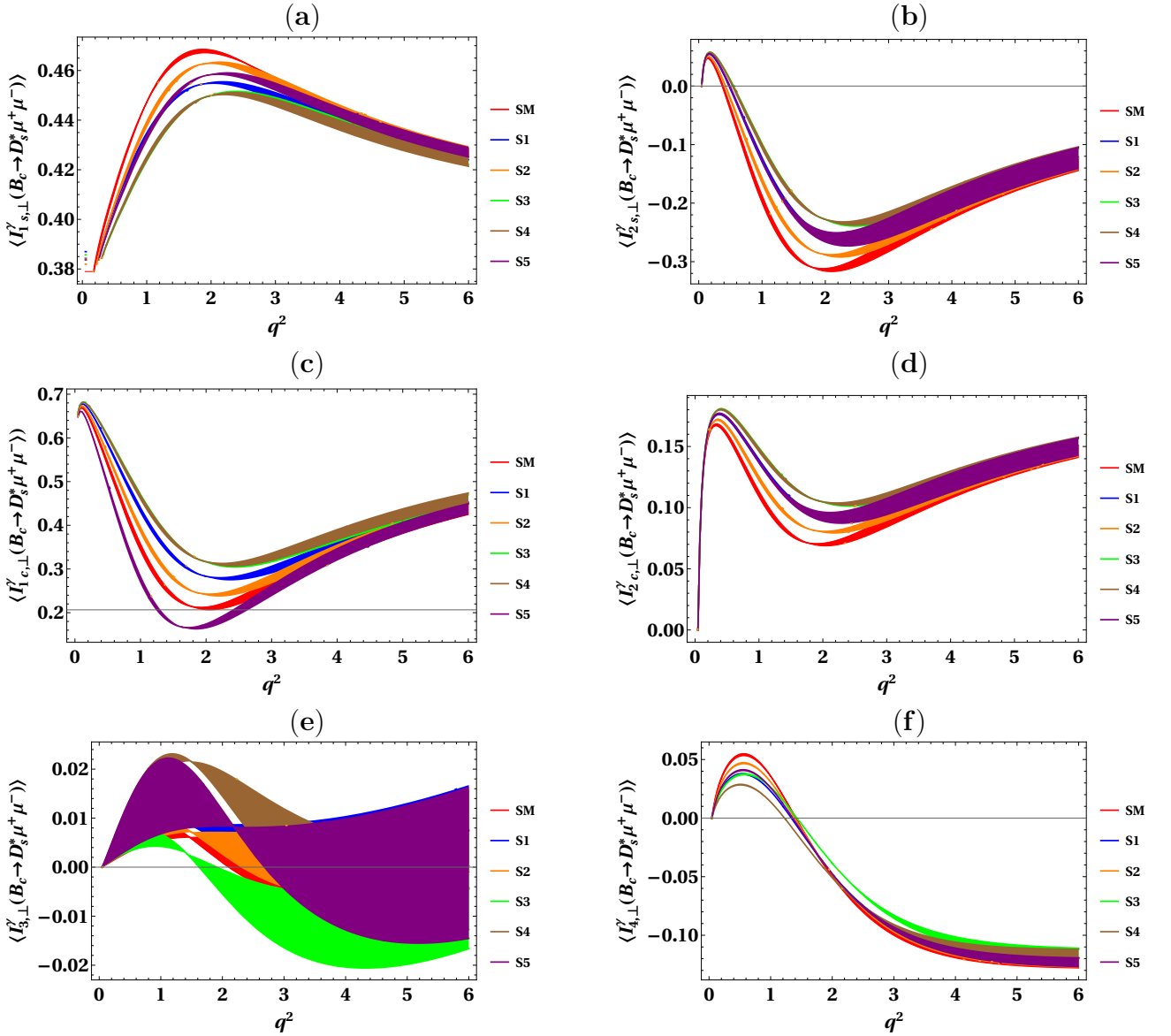


Figure 4: Angular observables  $\langle I_{1s,\perp}^\gamma \rangle$ ,  $\langle I_{2s,\perp}^\gamma \rangle$ ,  $\langle I_{1c,\perp}^\gamma \rangle$ ,  $\langle I_{2c,\perp}^\gamma \rangle$ ,  $\langle I_{3,\perp}^\gamma \rangle$ , and  $\langle I_{4,\perp}^\gamma \rangle$  for the decay  $B_c \rightarrow D_s^*(\rightarrow D_s \gamma) \mu^+ \mu^-$ , in the SM and the NP scenarios.

2D NP scenarios presented in Table 4. Numerical values of the SM and NP predictions of the averaged angular coefficients, with errors due to the form factors, in different  $q^2$  bins, are listed in Tables 12-18, of appendix B. We also show the results of the angular observables as a function of  $q^2$  in Figs. 4-7. We now discuss these results of angular observables.

- Fig. 4, shows the angular coefficients  $\langle I_{1s,\perp}^\gamma \rangle$ ,  $\langle I_{2s,\perp}^\gamma \rangle$ ,  $\langle I_{1c,\perp}^\gamma \rangle$ ,  $\langle I_{2c,\perp}^\gamma \rangle$ ,  $\langle I_{3,\perp}^\gamma \rangle$ , and  $\langle I_{4,\perp}^\gamma \rangle$  as a function of  $q^2$  both in the SM and in 1D and 2D NP scenarios. From Figs. 4(b), 4(c), 4(d), and 4(e), one can see that the angular observables  $\langle I_{2s,\perp}^\gamma \rangle$ ,  $\langle I_{1c,\perp}^\gamma \rangle$ ,  $\langle I_{2c,\perp}^\gamma \rangle$ , and  $\langle I_{3,\perp}^\gamma \rangle$  deviate significantly from the SM predictions at  $q^2 = [2, 3]$  GeV<sup>2</sup>. Furthermore these observables also discriminate the 1D and 2D NP scenarios at  $q^2 = [2, 3]$  GeV<sup>2</sup>. Similarly, the angular observables  $\langle I_{1s,\perp}^\gamma \rangle$  and  $\langle I_{4,\perp}^\gamma \rangle$  presented in Figs. 4(a), and 4(e) show a clear departure from the SM predictions and the 1D and 2D NP scenarios are discriminated around  $q^2 = [1, 2]$  GeV<sup>2</sup>.
- Fig. 5, depicts the angular coefficients  $\langle I_{5,\perp}^\gamma \rangle$ ,  $\langle I_{6s,\perp}^\gamma \rangle$ , and  $\langle I_{6c,\perp}^\gamma \rangle$  as a function of  $q^2$  both in the SM and in 1D and 2D NP scenarios. For  $\langle I_{5,\perp}^\gamma \rangle$  (cf. Fig. 5(a)), the value of zero crossing in the SM is  $q^2 \approx 2.5$  GeV<sup>2</sup>. The deviation of the zero crossing of  $\langle I_{5,\perp}^\gamma \rangle$  arises in the case of scenarios S2, S3, S4, and S5, but scenario S1 is not distinguishable. For the angular coefficients  $\langle I_{6s,\perp}^\gamma \rangle$  and  $\langle I_{6c,\perp}^\gamma \rangle$ , there is a shift in zero crossing compared to that of SM, with distinct zero crossing points for scenarios S2, S4, and S5. However, the scenarios S1 and S3 are not much distinguishable.
- Fig. 6, shows the angular coefficients  $\langle I_{1s,\parallel} \rangle$ ,  $\langle I_{2s,\parallel} \rangle$ ,  $\langle I_{1c,\parallel} \rangle$ , and  $\langle I_{2c,\parallel} \rangle$  for the decay  $B_c \rightarrow D_s^*(\rightarrow D_s\pi)\mu^+\mu^-$  in the SM and in NP scenarios S1, S2, S3, S4 and S5. The effects of NP are distinct compared to that of SM. For angular coefficients  $\langle I_{1s,\parallel} \rangle$ , and  $\langle I_{2s,\parallel} \rangle$  (cf.

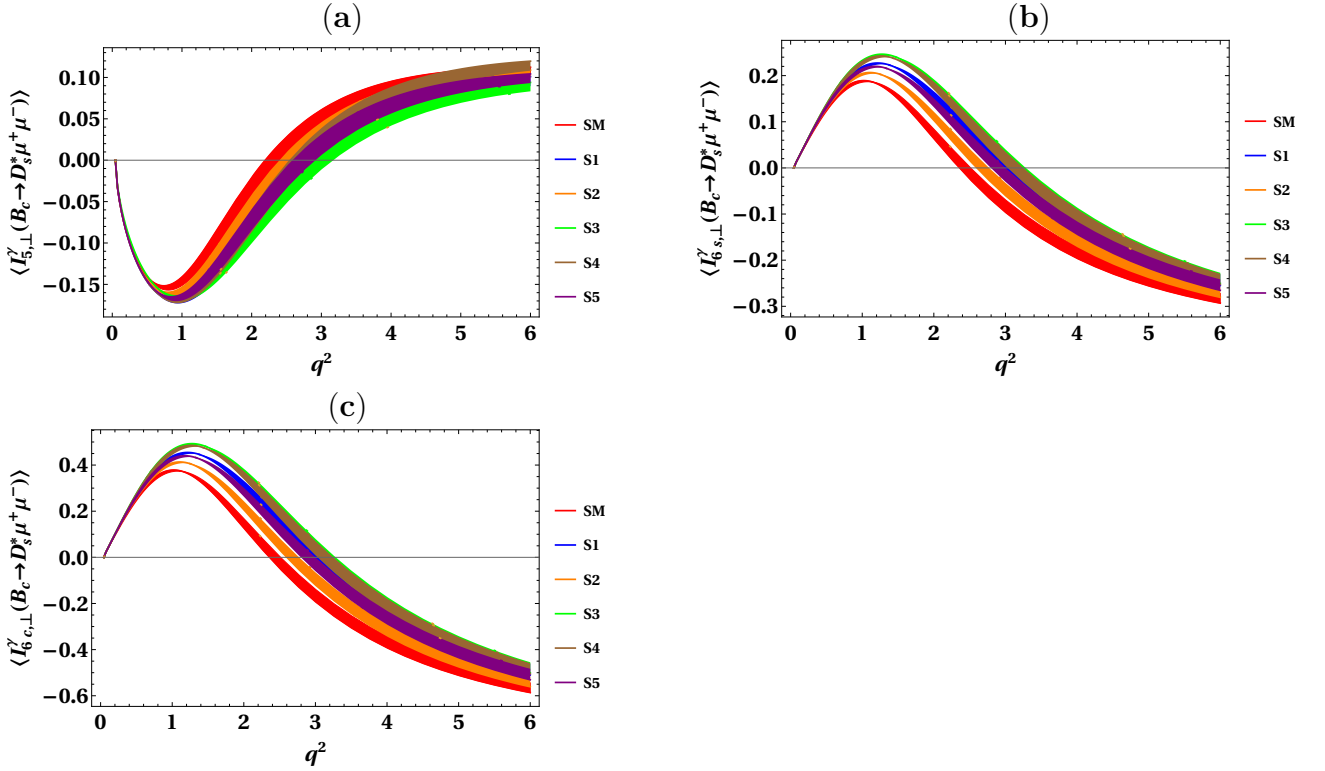


Figure 5: Angular observables  $\langle I_{5,\perp}^\gamma \rangle$ ,  $\langle I_{6s,\perp}^\gamma \rangle$ , and  $\langle I_{6c,\perp}^\gamma \rangle$  for the decay  $B_c \rightarrow D_s^*(\rightarrow D_s^*\gamma)\mu^+\mu^-$ , in the SM and the NP scenarios.

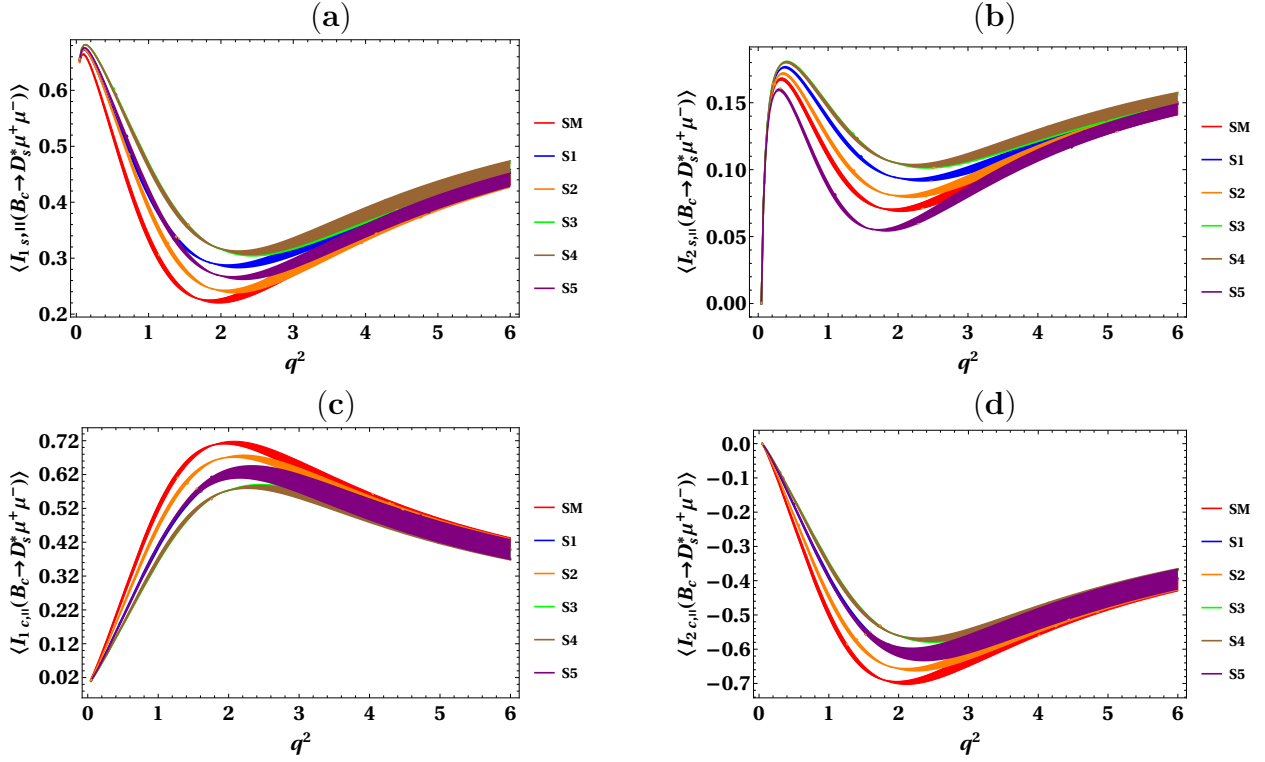


Figure 6: Angular observables  $\langle I_{1s,||} \rangle$ ,  $\langle I_{2s,||} \rangle$ ,  $\langle I_{1c,||} \rangle$ , and  $\langle I_{2c,||} \rangle$  for the decay  $B_c \rightarrow D_s^*(\rightarrow D_s^*\pi)\mu^+\mu^-$ , in the SM and the NP scenarios.

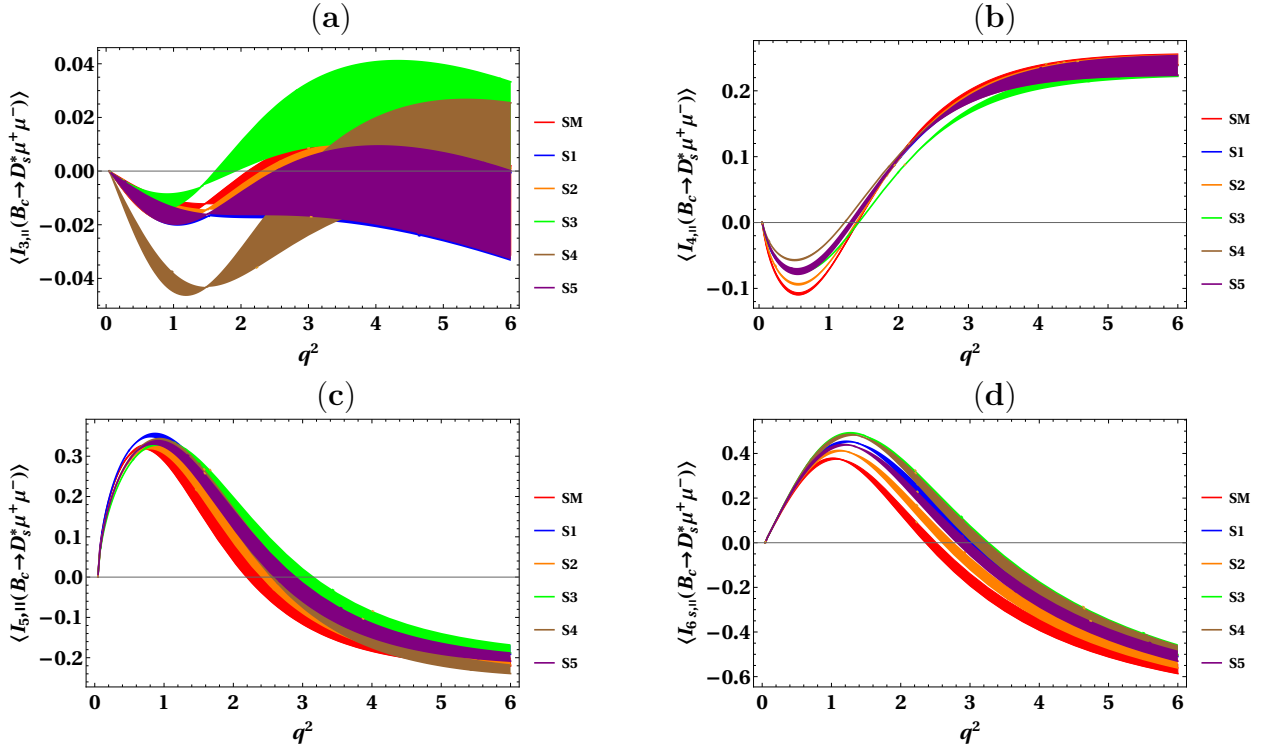


Figure 7: Angular observables  $\langle I_{3,||} \rangle$ ,  $\langle I_{4,||} \rangle$ ,  $\langle I_{5,||} \rangle$ , and  $\langle I_{6s,||} \rangle$  for the decay  $B_c \rightarrow D_s^*(\rightarrow D_s^*\pi)\mu^+\mu^-$ , in the SM and the NP scenarios.

Fig. 6(a,b)), the scenarios S1, S2, S4 and S5 are quite distinct in the kinematical region  $q^2 = [1, 2]$  GeV<sup>2</sup>. Similarly for the angular coefficients  $\langle I_{1c,||} \rangle$  and  $\langle I_{2c,||} \rangle$  (cf. Fig. 6(c,d)), the NP scenarios S2, S3 and S5 are quite distinct in the region  $q^2 = [1, 2]$  GeV<sup>2</sup>. However in the region  $q^2 = [3, 6]$  GeV<sup>2</sup> the angular coefficients  $\langle I_{1c,||} \rangle$ , and  $\langle I_{2c,||} \rangle$  for most of the NP scenarios overlap.

- In Fig. 7, we have plotted the angular coefficients  $\langle I_{3,||} \rangle$ ,  $\langle I_{4,||} \rangle$ ,  $\langle I_{5,||} \rangle$ , and  $\langle I_{6s,||} \rangle$  for the decay  $B_c \rightarrow D_s^*(\rightarrow D_s\pi)\mu^+\mu^-$ , in the framework of SM as well as NP scenarios. For the angular coefficients  $\langle I_{3,||} \rangle$ ,  $\langle I_{4,||} \rangle$ , and  $\langle I_{5,||} \rangle$  shown in Figs. 7(a), 7(b), and 7(c), respectively, the NP scenarios under consideration are discriminated in the region  $q^2 = [1, 2]$  GeV<sup>2</sup> and  $q^2 = [3, 4]$  GeV<sup>2</sup>, with uncertainties due to form factors negligibly small in the angular coefficient  $\langle I_{4,||} \rangle$ .

## 4 Conclusions

Study of rare semileptonic decays of  $B$  meson gives us a path to investigate physics beyond the SM. In literature various exclusive semileptonic decays mediated by the flavor changing neutral current transitions and flavor changing charged current transitions show reasonable deviations from the SM predictions. As various global fit analyses suggest the presence of NP, in different physical observables of  $B \rightarrow (K, K^*)\mu^+\mu^-$  decays, in terms of the fit values of the NP coupling, we analyze the implications of these NP scenarios onto the angular observables of the complementary four-fold  $B_c \rightarrow D_s^*(\rightarrow D_s\gamma, (D_s\pi))\mu^+\mu^-$  decays, which are governed by the same quark level transition. Using the effective Hamiltonian by incorporating the vector and axial-vector NP operators ( $O_9, O_{9'}, O_{10}, O_{10'}$ ), we have derived the four-fold angular distributions for  $B_c \rightarrow D_s^*(\rightarrow D_s\gamma)\mu^+\mu^-$ , and  $B_c \rightarrow D_s^*(\rightarrow D_s\pi)\mu^+\mu^-$  decays from which the individual angular coefficients and various physical observables can be extracted. To analyze the NP effects, in these observables, we use the best fit values of the Wilson coefficients coming from the global fit analysis with the assumption of NP present only in the muon sector.

To summarize our work, we have observed sizeable difference between the NP predictions of different physical observables and the angular coefficients for  $B_c \rightarrow D_s^*(\rightarrow D_s\gamma)\mu^+\mu^-$  and  $B_c \rightarrow D_s^*(\rightarrow D_s\pi)\mu^+\mu^-$  decays, compared to the SM expectations. The NP results of the differential branching ratios for the considered decays indicate decreased values compared to that of the SM, however due to large error bands coming from the errors due to the form factors, NP results remain compatible with the SM estimates. Considering the forward-backward asymmetry and the longitudinal helicity fraction of  $D_s^*$  meson, a number of NP scenarios can be distinguished from the SM predictions as well as from each other, in some kinematical ranges. For the unpolarized and polarized LFUV ratios i.e.  $R_{D_s^*}$  and  $R_{D_s^*}^{L,T}$ , our analysis shows that there is no sizeable deviations expected from the SM prediction. Furthermore, the NP analysis considering the individual angular coefficients also shows sizeable deviations from the SM predictions along with distinct predictions for different NP scenarios. Hence the precise measurement of the studied physical observables for  $B_c \rightarrow D_s^*(\rightarrow D_s\gamma)\mu^+\mu^-$ , and  $B_c \rightarrow D_s^*(\rightarrow D_s\pi)\mu^+\mu^-$  decays at LHCb and the future collider experiments will give useful complementary information, required to clarify the structure of new physics in  $b \rightarrow s\ell\ell$  decays.

## Acknowledgments

This work is supported by Higher Education Commission of Pakistan through Grant no. NRPU/20-15142.



## A SM Wilson Coefficients

The explicit expressions used for the Wilson coefficients are given as follows [51–56],

$$\begin{aligned}
C_7^{\text{eff}}(q^2) &= C_7 - \frac{1}{3} \left( C_3 + \frac{4}{3}C_4 + 20C_5 + \frac{80}{3}C_6 \right) - \frac{\alpha_s}{4\pi} \left[ (C_1 - 6C_2)F_{1,c}^{(7)}(q^2) + C_8F_8^{(7)}(q^2) \right], \\
C_9^{\text{eff}}(q^2) &= C_9 + \frac{4}{3} \left( C_3 + \frac{16}{3}C_5 + \frac{16}{9}C_6 \right) - h(0, q^2) \left( \frac{1}{2}C_3 + \frac{2}{3}C_4 + 8C_5 + \frac{32}{3}C_6 \right) \\
&\quad - h(m_b^{\text{pole}}, q^2) \left( \frac{7}{2}C_3 + \frac{2}{3}C_4 + 38C_5 + \frac{32}{3}C_6 \right) + h(m_c^{\text{pole}}, q^2) \left( \frac{4}{3}C_1 + C_2 + 6C_3 + 60C_5 \right) \\
&\quad - \frac{\alpha_s}{4\pi} \left[ C_1F_{1,c}^{(9)}(q^2) + C_2F_{2,c}^{(9)}(q^2) + C_8F_8^{(9)}(q^2) \right], \tag{53}
\end{aligned}$$

where the functions  $h(m_q^{\text{pole}}, q^2)$  with  $q = c, b$ , and functions  $F_8^{(7,9)}(q^2)$  are defined in [52], while the functions  $F_{1,c}^{(7,9)}(q^2)$ ,  $F_{2,c}^{(7,9)}(q^2)$  are given in [54] for low  $q^2$  and in [55] for high  $q^2$ . The quark masses appearing in all of these functions are defined in the pole scheme.

## B Binned Predictions of Physical Observables

In this appendix, we give the SM as well as NP predictions of physical observables in different  $q^2$  bins.

Table 5: Predictions of averaged values of observables such as differential branching ratios,  $d\mathcal{B}(B_c \rightarrow D_s^* \mu^+ \mu^-)/dq^2$ ,  $d\mathcal{B}(B_c \rightarrow D_s^*(\rightarrow D_s \pi) \mu^+ \mu^-)/dq^2$ ,  $d\mathcal{B}(B_c \rightarrow D_s^*(\rightarrow D_s \gamma) \mu^+ \mu^-)/dq^2$ , longitudinal helicity fraction  $f_L$ , lepton forward-backward asymmetry  $A_{FB}$ , unpolarized LFUV ratio  $R_{D_s^*}$ , and polarized LFUV ratios  $R_{D_s^*}^{L,T}$ , in  $q^2 = [0.045 - 1.0]$  GeV<sup>2</sup> bin, for the SM as well as the NP scenarios presented in Table 4. The listed errors arise due to the uncertainties of the form factors.

$q^2 = [0.045 - 1.0]$ GeV <sup>2</sup>						
Observables	SM	S1	S2	S3	S4	S5
$\frac{d\mathcal{B}}{dq^2}(B_c \rightarrow D_s^* \mu^+ \mu^-) \times 10^8$	$5.013_{-0.476}^{+0.554}$	$5.041_{-0.558}^{+0.480}$	$5.041_{-0.471}^{+0.463}$	$5.041_{-0.458}^{+0.480}$	$5.040_{-0.458}^{+0.476}$	$5.047_{-0.469}^{+0.468}$
$\frac{d\mathcal{B}}{dq^2}(B_c \rightarrow D_s^*(\rightarrow D_s \pi) \mu^+ \mu^-) \times 10^{10}$	$2.61_{-0.24}^{+0.23}$	$2.62_{-0.24}^{+0.25}$	$2.61_{-0.24}^{+0.25}$	$2.62_{-0.24}^{+0.25}$	$2.62_{-0.24}^{+0.25}$	$2.62_{-0.24}^{+0.25}$
$\frac{d\mathcal{B}}{dq^2}(B_c \rightarrow D_s^*(\rightarrow D_s \gamma) \mu^+ \mu^-) \times 10^8$	$2.760_{-0.253}^{+0.290}$	$2.781_{-0.250}^{+0.270}$	$2.948_{-0.238}^{+0.255}$	$2.750_{-0.253}^{+0.267}$	$2.752_{-0.247}^{+0.270}$	$2.734_{-0.251}^{+0.263}$
$f_L$	$0.175_{-0.004}^{+0.004}$	$0.135_{-0.004}^{+0.003}$	$0.156_{-0.004}^{+0.002}$	$0.118_{-0.003}^{+0.003}$	$0.119_{-0.003}^{+0.003}$	$0.141_{-0.003}^{+0.003}$
$A_{FB}$	$0.114_{-0.003}^{+0.003}$	$0.120_{-0.004}^{+0.003}$	$0.117_{-0.003}^{+0.003}$	$0.122_{-0.004}^{+0.004}$	$0.122_{-0.004}^{+0.003}$	$0.119_{-0.004}^{+0.003}$
$R_{D_s^*}$	$0.939_{-0.001}^{+0.001}$	$0.935_{-0.001}^{+0.001}$	$0.934_{-0.001}^{+0.001}$	$0.934_{-0.001}^{+0.001}$	$0.934_{-0.001}^{+0.001}$	$0.934_{-0.001}^{+0.001}$
$R_{D_s^*}^L$	$0.942_{-0.002}^{+0.002}$	$0.943_{-0.003}^{+0.003}$	$0.941_{-0.004}^{+0.003}$	$0.941_{-0.003}^{+0.003}$	$0.942_{-0.002}^{+0.003}$	$0.941_{-0.002}^{+0.003}$
$R_{D_s^*}^T$	$0.933_{-0.001}^{+0.001}$	$0.934_{-0.001}^{+0.001}$	$0.932_{-0.001}^{+0.001}$	$0.933_{-0.001}^{+0.001}$	$0.933_{-0.001}^{+0.001}$	$0.933_{-0.001}^{+0.001}$



Table 6: Same as in Table 5, but for  $q^2 = [1.0 - 2.0]$  GeV<sup>2</sup> bin.

$q^2 = [1.0 - 2.0]$ GeV <sup>2</sup>						
Observables	SM	S1	S2	S3	S4	S5
$\frac{d\mathcal{B}}{dq^2}(B_c \rightarrow D_s^* \mu^+ \mu^-) \times 10^8$	$0.938^{+0.114}_{-0.105}$	$0.887^{+0.103}_{-0.096}$	$0.905^{+0.108}_{-0.099}$	$0.843^{+0.099}_{-0.089}$	$0.848^{+0.090}_{-0.098}$	$0.893^{+0.103}_{-0.098}$
$\frac{d\mathcal{B}}{dq^2}(B_c \rightarrow D_s^*(\rightarrow D_s \pi) \mu^+ \mu^-) \times 10^{10}$	$4.880^{+0.059}_{-0.050}$	$5.150^{+0.032}_{-0.040}$	$5.270^{+0.060}_{-0.094}$	$3.910^{+0.900}_{-0.800}$	$3.940^{+0.050}_{-0.060}$	$4.940^{+0.026}_{-0.080}$
$\frac{d\mathcal{B}}{dq^2}(B_c \rightarrow D_s^*(\rightarrow D_s \gamma) \mu^+ \mu^-) \times 10^8$	$1.032^{+0.128}_{-0.118}$	$3.980^{+0.118}_{-0.109}$	$0.876^{+0.097}_{-0.106}$	$0.932^{+0.113}_{-0.105}$	$0.942^{+0.114}_{-0.104}$	$0.918^{+0.110}_{-0.101}$
$f_L$	$0.661^{+0.004}_{-0.006}$	$0.542^{+0.005}_{-0.007}$	$0.606^{+0.005}_{-0.005}$	$0.496^{+0.004}_{-0.004}$	$0.497^{+0.002}_{-0.006}$	$0.564^{+0.006}_{-0.006}$
$A_{FB}$	$0.221^{+0.0007}_{-0.008}$	$0.311^{+0.002}_{-0.002}$	$0.265^{+0.005}_{-0.006}$	$0.343^{+0.001}_{-0.001}$	$0.337^{+0.002}_{-0.002}$	$0.296^{+0.003}_{-0.004}$
$R_{D_s^*}$	$0.989^{+0.001}_{-0.001}$	$0.990^{+0.001}_{-0.001}$	$0.989^{+0.001}_{-0.001}$	$0.989^{+0.001}_{-0.001}$	$0.988^{+0.001}_{-0.001}$	$0.989^{+0.001}_{-0.001}$
$R_{D_s^*}^L$	$0.997^{+0.001}_{-0.001}$	$0.996^{+0.001}_{-0.001}$	$0.997^{+0.001}_{-0.001}$	$0.997^{+0.001}_{-0.001}$	$0.996^{+0.001}_{-0.001}$	$0.997^{+0.001}_{-0.001}$
$R_{D_s^*}^T$	$0.973^{+0.002}_{-0.002}$	$0.978^{+0.001}_{-0.001}$	$0.977^{+0.001}_{-0.001}$	$0.981^{+0.001}_{-0.001}$	$0.981^{+0.001}_{-0.001}$	$0.979^{+0.002}_{-0.001}$

 Table 7: Same as in Table 5, but for  $q^2 = [2.0 - 3.0]$  GeV<sup>2</sup> bin.

$q^2 = [2.0 - 3.0]$ GeV <sup>2</sup>						
Observables	SM	S1	S2	S3	S4	S5
$\frac{d\mathcal{B}}{dq^2}(B_c \rightarrow D_s^* \mu^+ \mu^-) \times 10^8$	$1.091^{+0.172}_{-0.154}$	$0.932^{+0.142}_{-0.127}$	$1.004^{+0.156}_{-0.136}$	$0.864^{+0.134}_{-0.120}$	$0.875^{+0.134}_{-0.120}$	$0.927^{+0.172}_{-0.104}$
$\frac{d\mathcal{B}}{dq^2}(B_c \rightarrow D_s^*(\rightarrow D_s \pi) \mu^+ \mu^-) \times 10^{10}$	$5.607^{+0.090}_{-0.080}$	$5.580^{+0.050}_{-0.035}$	$6.030^{+0.050}_{-0.030}$	$3.870^{+1.030}_{-0.087}$	$3.930^{+0.050}_{-0.060}$	$5.410^{+0.034}_{-0.098}$
$\frac{d\mathcal{B}}{dq^2}(B_c \rightarrow D_s^*(\rightarrow D_s \gamma) \mu^+ \mu^-) \times 10^8$	$1.229^{+0.172}_{-0.193}$	$1.079^{+0.164}_{-0.147}$	$0.968^{+0.149}_{-0.133}$	$1.007^{+0.156}_{-0.140}$	$1.020^{+0.161}_{-0.137}$	$1.003^{+0.153}_{-0.137}$
$f_L$	$0.691^{+0.011}_{-0.011}$	$0.622^{+0.006}_{-0.007}$	$0.663^{+0.040}_{-0.054}$	$0.586^{+0.005}_{-0.010}$	$0.581^{+0.006}_{-0.006}$	$0.637^{+0.007}_{-0.007}$
$A_{FB}$	$-0.020^{+0.018}_{-0.019}$	$0.116^{+0.014}_{-0.017}$	$0.039^{+0.020}_{-0.018}$	$0.156^{+0.016}_{-0.019}$	$0.160^{+0.020}_{-0.018}$	$0.089^{+0.108}_{-0.071}$
$R_{D_s^*}$	$0.989^{+0.001}_{-0.001}$	$0.988^{+0.001}_{-0.001}$	$0.989^{+0.001}_{-0.001}$	$0.988^{+0.001}_{-0.001}$	$0.988^{+0.001}_{-0.001}$	$0.989^{+0.001}_{-0.001}$
$R_{D_s^*}^L$	$0.997^{+0.001}_{-0.001}$	$0.996^{+0.001}_{-0.001}$	$0.997^{+0.001}_{-0.001}$	$0.997^{+0.001}_{-0.001}$	$0.996^{+0.001}_{-0.001}$	$0.997^{+0.001}_{-0.001}$
$R_{D_s^*}^T$	$0.974^{+0.001}_{-0.001}$	$0.974^{+0.001}_{-0.001}$	$0.974^{+0.001}_{-0.001}$	$0.976^{+0.001}_{-0.001}$	$0.976^{+0.001}_{-0.001}$	$0.975^{+0.001}_{-0.001}$

 Table 8: Same as in Table 5, but for  $q^2 = [3.0 - 4.0]$  GeV<sup>2</sup> bin.

$q^2 = [3.0 - 4.0]$ GeV <sup>2</sup>						
Observables	SM	S1	S2	S3	S4	S5
$\frac{d\mathcal{B}}{dq^2}(B_c \rightarrow D_s^* \mu^+ \mu^-) \times 10^8$	$1.537^{+0.281}_{-0.245}$	$1.248^{+0.222}_{-0.195}$	$1.248^{+0.386}_{-0.083}$	$1.150^{+0.210}_{-0.184}$	$1.167^{+0.169}_{-0.189}$	$1.522^{+0.580}_{-0.293}$
$\frac{d\mathcal{B}}{dq^2}(B_c \rightarrow D_s^*(\rightarrow D_s \pi) \mu^+ \mu^-) \times 10^{10}$	$7.990^{+0.146}_{-0.127}$	$7.650^{+0.087}_{-0.201}$	$8.500^{+0.156}_{-0.178}$	$5.020^{+0.200}_{-0.198}$	$5.100^{+0.156}_{-0.189}$	$7.570^{+0.345}_{-0.321}$
$\frac{d\mathcal{B}}{dq^2}(B_c \rightarrow D_s^*(\rightarrow D_s \gamma) \mu^+ \mu^-) \times 10^8$	$1.723^{+0.272}_{-0.310}$	$1.448^{+0.220}_{-0.255}$	$1.330^{+0.239}_{-0.210}$	$1.134^{+0.342}_{-0.140}$	$1.370^{+0.246}_{-0.216}$	$1.355^{+0.241}_{-0.211}$
$f_L$	$0.595^{+0.018}_{-0.016}$	$0.565^{+0.025}_{-0.015}$	$0.584^{+0.030}_{-0.015}$	$0.538^{+0.040}_{-0.019}$	$0.528^{+0.016}_{-0.016}$	$0.572^{+0.016}_{-0.014}$
$A_{FB}$	$-0.212^{+0.008}_{-0.022}$	$-0.093^{+0.026}_{-0.024}$	$-0.164^{+0.017}_{-0.020}$	$-0.063^{+0.024}_{-0.019}$	$-0.145^{+0.025}_{-0.015}$	$-0.120^{+0.020}_{-0.023}$
$R_{D_s^*}$	$0.991^{+0.001}_{-0.001}$	$0.988^{+0.001}_{-0.001}$	$0.991^{+0.001}_{-0.001}$	$0.990^{+0.001}_{-0.001}$	$0.989^{+0.001}_{-0.001}$	$0.990^{+0.001}_{-0.001}$
$R_{D_s^*}^L$	$0.997^{+0.001}_{-0.001}$	$0.996^{+0.002}_{-0.002}$	$0.997^{+0.002}_{-0.001}$	$0.997^{+0.001}_{-0.001}$	$0.996^{+0.001}_{-0.001}$	$0.997^{+0.002}_{-0.001}$
$R_{D_s^*}^T$	$0.983^{+0.002}_{-0.002}$	$0.981^{+0.002}_{-0.003}$	$0.982^{+0.001}_{-0.002}$	$0.981^{+0.001}_{-0.001}$	$0.981^{+0.001}_{-0.001}$	$0.982^{+0.001}_{-0.001}$

 Table 9: Same as in Table 5, but for  $q^2 = [4.0 - 5.0]$  GeV<sup>2</sup> bin.

$q^2 = [4.0 - 5.0]$ GeV <sup>2</sup>						
Observables	SM	S1	S2	S3	S4	S5
$\frac{d\mathcal{B}}{dq^2}(B_c \rightarrow D_s^* \mu^+ \mu^-) \times 10^8$	$2.187^{+0.445}_{-0.381}$	$1.733^{+0.347}_{-0.298}$	$1.733^{+0.612}_{-0.120}$	$1.596^{+0.328}_{-0.281}$	$1.621^{+0.333}_{-0.285}$	$1.670^{+0.494}_{-0.179}$
$\frac{d\mathcal{B}}{dq^2}(B_c \rightarrow D_s^*(\rightarrow D_s \pi) \mu^+ \mu^-) \times 10^{10}$	$1.137^{+0.232}_{-0.201}$	$1.080^{+0.340}_{-0.321}$	$1.220^{+0.296}_{-0.281}$	$0.684^{+0.316}_{-0.350}$	$0.695^{+0.300}_{-0.234}$	$1.023^{+0.212}_{-0.345}$
$\frac{d\mathcal{B}}{dq^2}(B_c \rightarrow D_s^*(\rightarrow D_s \gamma) \mu^+ \mu^-) \times 10^8$	$2.434^{+0.490}_{-0.418}$	$1.999^{+0.341}_{-0.395}$	$1.875^{+0.376}_{-0.324}$	$1.858^{+0.376}_{-0.323}$	$1.892^{+0.381}_{-0.328}$	$1.887^{+0.376}_{-0.323}$
$f_L$	$0.508^{+0.018}_{-0.017}$	$0.494^{+0.016}_{-0.016}$	$0.503^{+0.023}_{-0.420}$	$0.474^{+0.013}_{-0.020}$	$0.461^{+0.018}_{-0.018}$	$0.497^{+0.017}_{-0.016}$
$A_{FB}$	$-0.329^{+0.016}_{-0.020}$	$-0.237^{+0.019}_{-0.019}$	$-0.294^{+0.018}_{-0.020}$	$-0.215^{+0.025}_{-0.015}$	$-0.225^{+0.020}_{-0.021}$	$-0.260^{+0.018}_{-0.022}$
$R_{D_s^*}$	$0.993^{+0.001}_{-0.001}$	$0.989^{+0.001}_{-0.001}$	$0.992^{+0.001}_{-0.001}$	$0.991^{+0.001}_{-0.001}$	$0.991^{+0.001}_{-0.002}$	$0.992^{+0.002}_{-0.002}$
$R_{D_s^*}^L$	$0.997^{+0.001}_{-0.001}$	$0.996^{+0.002}_{-0.002}$	$0.997^{+0.001}_{-0.001}$	$0.997^{+0.001}_{-0.002}$	$0.996^{+0.001}_{-0.001}$	$0.997^{+0.001}_{-0.001}$
$R_{D_s^*}^T$	$0.988^{+0.001}_{-0.001}$	$0.986^{+0.001}_{-0.001}$	$0.988^{+0.001}_{-0.001}$	$0.986^{+0.001}_{-0.001}$	$0.987^{+0.001}_{-0.001}$	$0.987^{+0.001}_{-0.001}$

Table 10: Same as in Table 5, but for  $q^2 = [5.0 - 6.0]$  GeV<sup>2</sup> bin.

$q^2 = [5.0 - 6.0]$ GeV <sup>2</sup>						
Observables	SM	S1	S2	S3	S4	S5
$\frac{d\mathcal{B}}{dq^2}(B_c \rightarrow D_s^* \mu^+ \mu^-) \times 10^8$	$3.056^{+0.683}_{-0.574}$	$2.391^{+0.529}_{-0.446}$	$2.391^{+0.990}_{-0.186}$	$2.204^{+0.500}_{-0.419}$	$2.237^{+0.508}_{-0.427}$	$2.341^{+0.708}_{-0.312}$
$\frac{d\mathcal{B}}{dq^2}(B_c \rightarrow D_s^*(\rightarrow D_s \pi) \mu^+ \mu^-) \times 10^{10}$	$1.589^{+0.355}_{-0.298}$	$1.519^{+0.476}_{-0.507}$	$1.785^{+0.500}_{-0.494}$	$9.281^{+0.480}_{-0.478}$	$9.422^{+0.450}_{-0.480}$	$1.407^{+0.389}_{-0.283}$
$\frac{d\mathcal{B}}{dq^2}(B_c \rightarrow D_s^*(\rightarrow D_s \gamma) \mu^+ \mu^-) \times 10^8$	$3.379^{+0.745}_{-0.628}$	$2.740^{+0.599}_{-0.505}$	$2.610^{+0.578}_{-0.487}$	$2.548^{+0.569}_{-0.479}$	$2.593^{+0.577}_{-0.486}$	$2.608^{+0.559}_{-0.487}$
$f_L$	$0.442^{+0.060}_{-0.025}$	$0.435^{+0.052}_{-0.019}$	$0.440^{+0.060}_{-0.024}$	$0.421^{+0.430}_{-0.395}$	$0.406^{+0.424}_{-0.424}$	$0.437^{+0.054}_{-0.021}$
$A_{FB}$	$-0.400^{+0.015}_{-0.017}$	$-0.332^{+0.017}_{-0.019}$	$-0.376^{+0.016}_{-0.019}$	$-0.316^{+0.024}_{-0.013}$	$-0.327^{+0.017}_{-0.020}$	$-0.350^{+0.017}_{-0.021}$
$R_{D_s^*}$	$0.992^{+0.002}_{-0.002}$	$0.991^{+0.002}_{-0.002}$	$0.994^{+0.002}_{-0.002}$	$0.993^{+0.002}_{-0.002}$	$0.993^{+0.002}_{-0.002}$	$0.993^{+0.002}_{-0.002}$
$R_{D_s^*}^L$	$0.997^{+0.001}_{-0.001}$	$0.996^{+0.001}_{-0.001}$	$0.997^{+0.001}_{-0.001}$	$0.997^{+0.001}_{-0.002}$	$0.996^{+0.001}_{-0.002}$	$0.997^{+0.001}_{-0.002}$
$R_{D_s^*}^T$	$0.991^{+0.001}_{-0.001}$	$0.990^{+0.001}_{-0.002}$	$0.991^{+0.001}_{-0.002}$	$0.990^{+0.001}_{-0.001}$	$0.990^{+0.001}_{-0.002}$	$0.990^{+0.001}_{-0.001}$

 Table 11: Same as in Table 5, but for  $q^2 = [1.0 - 6.0]$  GeV<sup>2</sup> bin.

$q^2 = [1.0 - 6.0]$ GeV <sup>2</sup>						
Observables	SM	S1	S2	S3	S4	S5
$\frac{d\mathcal{B}}{dq^2}(B_c \rightarrow D_s^* \mu^+ \mu^-) \times 10^8$	$2.106^{+0.455}_{-0.384}$	$1.659^{+0.349}_{-0.294}$	$1.659^{+0.616}_{-0.124}$	$1.529^{+0.330}_{-0.277}$	$1.552^{+0.335}_{-0.280}$	$1.626^{+0.468}_{-0.208}$
$\frac{d\mathcal{B}}{dq^2}(B_c \rightarrow D_s^*(\rightarrow D_s \pi) \mu^+ \mu^-) \times 10^{10}$	$1.095^{+0.237}_{-0.199}$	$1.040^{+0.303}_{-0.331}$	$9.740^{+0.209}_{-0.300}$	$7.806^{+0.860}_{-0.296}$	$8.073^{+0.740}_{-0.461}$	$9.759^{+0.131}_{-0.384}$
$\frac{d\mathcal{B}}{dq^2}(B_c \rightarrow D_s^*(\rightarrow D_s \gamma) \mu^+ \mu^-) \times 10^8$	$9.797^{+0.863}_{-0.613}$	$8.246^{+0.532}_{-0.520}$	$7.657^{+0.448}_{-0.249}$	$7.691^{+0.457}_{-0.260}$	$7.521^{+0.475}_{-0.276}$	$7.821^{+0.452}_{-0.256}$
$f_L$	$0.539^{+0.056}_{-0.023}$	$0.509^{+0.523}_{-0.496}$	$0.528^{+0.056}_{-0.013}$	$0.485^{+0.093}_{-0.065}$	$0.475^{+0.089}_{-0.061}$	$0.516^{+0.030}_{-0.002}$
$A_{FB}$	$-0.236^{+0.020}_{-0.026}$	$-0.130^{+0.023}_{-0.026}$	$-0.194^{+0.023}_{-0.024}$	$-0.101^{+0.029}_{-0.020}$	$-0.171^{+0.022}_{-0.25}$	$-0.154^{+0.023}_{-0.024}$
$R_{D_s^*}$	$0.993^{+0.001}_{-0.001}$	$0.993^{+0.001}_{-0.001}$	$0.992^{+0.001}_{-0.001}$	$0.991^{+0.001}_{-0.001}$	$0.991^{+0.001}_{-0.001}$	$0.991^{+0.002}_{-0.002}$
$R_{D_s^*}^L$	$0.997^{+0.002}_{-0.002}$	$0.997^{+0.001}_{-0.002}$	$0.997^{+0.001}_{-0.002}$	$0.997^{+0.001}_{-0.001}$	$0.996^{+0.001}_{-0.001}$	$0.997^{+0.001}_{-0.001}$
$R_{D_s^*}^T$	$0.985^{+0.001}_{-0.001}$	$0.984^{+0.001}_{-0.001}$	$0.985^{+0.001}_{-0.001}$	$0.984^{+0.001}_{-0.001}$	$0.985^{+0.002}_{-0.002}$	$0.985^{+0.002}_{-0.002}$

 Table 12: Predictions of averaged values of the angular coefficients for the  $B_c \rightarrow D_s^*(\rightarrow D_s \pi) \mu^+ \mu^-$ , and  $B_c \rightarrow D_s^*(\rightarrow D_s \gamma) \mu^+ \mu^-$  decay, in  $q^2 = [0.045 - 1]$  GeV<sup>2</sup> bin, for the SM as well as the NP scenarios presented in Table-4. The listed errors arise due to the uncertainties of the form factors.

$q^2 = [0.045 - 1]$ GeV <sup>2</sup>												
Angular observables	SM		S1		S2		S3		S4		S5	
	$D_s \pi$	$D_s \gamma$	$D_s \pi$	$D_s \gamma$	$D_s \pi$	$D_s \gamma$	$D_s \pi$	$D_s \gamma$	$D_s \pi$	$D_s \gamma$	$D_s \pi$	$D_s \gamma$
$\langle I_{1s,i} \rangle, \langle I'_{1s,\perp} \rangle$	$0.580^{+0.003}_{-0.03}$	$0.391^{+0.001}_{-0.001}$	$0.610^{+0.003}_{-0.003}$	$0.386^{+0.001}_{-0.001}$	$0.608^{+0.003}_{-0.002}$	$0.387^{+0.001}_{-0.001}$	$0.635^{+0.002}_{-0.001}$	$0.389^{+0.002}_{-0.001}$	$0.635^{+0.002}_{-0.002}$	$0.384^{+0.001}_{-0.000}$	$0.619^{+0.003}_{-0.003}$	$0.386^{+0.001}_{-0.000}$
$\langle I_{2s,i} \rangle, \langle I'_{2s,\perp} \rangle$	$0.129^{+0.001}_{-0.001}$	$-0.015^{+0.003}_{-0.002}$	$0.137^{+0.002}_{-0.002}$	$0.005^{+0.002}_{-0.002}$	$0.135^{+0.001}_{-0.001}$	$0.004^{+0.002}_{-0.002}$	$0.141^{+0.002}_{-0.001}$	$0.0014^{+0.002}_{-0.002}$	$0.142^{+0.002}_{-0.002}$	$0.013^{+0.001}_{-0.001}$	$0.138^{+0.001}_{-0.001}$	$0.007^{+0.001}_{-0.001}$
$\langle I_{1c,i} \rangle, \langle I'_{1c,\perp} \rangle$	$0.205^{+0.004}_{-0.003}$	$0.580^{+0.003}_{-0.003}$	$0.163^{+0.003}_{-0.004}$	$0.610^{+0.003}_{-0.003}$	$0.164^{+0.004}_{-0.004}$	$0.608^{+0.003}_{-0.002}$	$0.124^{+0.023}_{-0.010}$	$0.635^{+0.002}_{-0.001}$	$0.0129^{+0.015}_{-0.013}$	$0.635^{+0.002}_{-0.002}$	$0.155^{+0.007}_{-0.005}$	$0.619^{+0.003}_{-0.003}$
$\langle I_{2c,i} \rangle, \langle I'_{2c,\perp} \rangle$	$-0.157^{+0.006}_{-0.002}$	$0.129^{+0.001}_{-0.001}$	$-0.127^{+0.003}_{-0.003}$	$0.137^{+0.002}_{-0.001}$	$-0.127^{+0.020}_{-0.013}$	$0.135^{+0.001}_{-0.001}$	$-0.097^{+0.012}_{-0.013}$	$0.141^{+0.002}_{-0.001}$	$-0.098^{+0.013}_{-0.010}$	$0.142^{+0.001}_{-0.002}$	$-0.116^{+0.005}_{-0.005}$	$0.138^{+0.001}_{-0.001}$
$\langle I_{3,i} \rangle, \langle I'_{3,\perp} \rangle$	$-0.006^{+0.002}_{-0.002}$	$0.003^{+0.000}_{-0.001}$	$-0.006^{+0.002}_{-0.002}$	$0.004^{+0.000}_{-0.002}$	$-0.006^{+0.002}_{-0.002}$	$0.003^{+0.001}_{-0.001}$	$-0.005^{+0.001}_{-0.002}$	$0.002^{+0.000}_{-0.000}$	$-0.015^{+0.001}_{-0.003}$	$0.007^{+0.001}_{-0.001}$	$-0.006^{+0.002}_{-0.002}$	$0.003^{+0.001}_{-0.001}$
$\langle I_{4,i} \rangle, \langle I'_{4,\perp} \rangle$	$-0.062^{+0.001}_{-0.002}$	$0.031^{+0.000}_{-0.001}$	$-0.042^{+0.001}_{-0.001}$	$0.020^{+0.000}_{-0.001}$	$-0.059^{+0.001}_{-0.001}$	$0.029^{+0.001}_{-0.001}$	$-0.042^{+0.004}_{-0.001}$	$0.021^{+0.000}_{-0.000}$	$-0.036^{+0.001}_{-0.006}$	$0.015^{+0.001}_{-0.000}$	$-0.050^{+0.002}_{-0.002}$	$0.024^{+0.001}_{-0.000}$
$\langle I_{5,i} \rangle, \langle I'_{5,\perp} \rangle$	$0.206^{+0.001}_{-0.001}$	$-0.103^{+0.000}_{-0.000}$	$0.215^{+0.001}_{-0.001}$	$-0.107^{+0.001}_{-0.000}$	$0.193^{+0.001}_{-0.001}$	$-0.096^{+0.001}_{-0.000}$	$0.186^{+0.001}_{-0.001}$	$-0.103^{+0.006}_{-0.000}$	$0.214^{+0.006}_{-0.014}$	$-0.107^{+0.000}_{-0.000}$	$0.195^{+0.009}_{-0.000}$	$-0.102^{+0.000}_{-0.000}$
$\langle I_{6s,i} \rangle, \langle I'_{6s,\perp} \rangle$	$0.152^{+0.004}_{-0.004}$	$0.083^{+0.002}_{-0.002}$	$0.160^{+0.004}_{-0.004}$	$0.087^{+0.003}_{-0.002}$	$0.156^{+0.005}_{-0.004}$	$0.078^{+0.000}_{-0.001}$	$0.163^{+0.005}_{-0.005}$	$0.089^{+0.003}_{-0.003}$	$0.163^{+0.004}_{-0.005}$	$0.089^{+0.003}_{-0.003}$	$0.158^{+0.005}_{-0.004}$	$0.083^{+0.002}_{-0.002}$
$\langle I_{6c,i} \rangle, \langle I'_{6c,\perp} \rangle$	0	$0.166^{+0.004}_{-0.004}$	0	$0.175^{+0.004}_{-0.004}$	0	$0.156^{+0.004}_{-0.004}$	0	$0.178^{+0.005}_{-0.006}$	0	$0.178^{+0.005}_{-0.006}$	0	$0.166^{+0.004}_{-0.005}$

 Table 13: Same as in Table 12, but for  $q^2 = [1.0 - 2.0]$  GeV<sup>2</sup> bin.

$q^2 = [1 - 2]$ GeV <sup>2</sup>												
Angular observables	SM		S1		S2		S3		S4		S5	
	$D_s \pi$	$D_s \gamma$	$D_s \pi$	$D_s \gamma$	$D_s \pi$	$D_s \gamma$	$D_s \pi$	$D_s \gamma$	$D_s \pi$	$D_s \gamma$	$D_s \pi$	$D_s \gamma$
$\langle I_{1s,i} \rangle, \langle I'_{1s,\perp} \rangle$	$0.253^{+0.005}_{-0.003}$	$0.461^{+0.001}_{-0.001}$	$0.343^{+0.004}_{-0.006}$	$0.448^{+0.001}_{-0.001}$	$0.294^{+0.005}_{-0.004}$	$0.455^{+0.001}_{-0.001}$	$0.377^{+0.004}_{-0.003}$	$0.442^{+0.001}_{-0.001}$	$0.376^{+0.004}_{-0.005}$	$0.443^{+0.001}_{-0.001}$	$0.326^{+0.005}_{-0.004}$	$0.450^{+0.001}_{-0.000}$
$\langle I_{2s,i} \rangle, \langle I'_{2s,\perp} \rangle$	$0.083^{+0.004}_{-0.002}$	$-0.274^{+0.002}_{-0.002}$	$0.111^{+0.013}_{-0.013}$	$-0.212^{+0.002}_{-0.003}$	$0.096^{+0.007}_{-0.005}$	$-0.242^{+0.003}_{-0.004}$	$0.122^{+0.002}_{-0.002}$	$-0.187^{+0.002}_{-0.003}$	$0.119^{+0.004}_{-0.008}$	$-0.189^{+0.002}_{-0.003}$	$0.106^{+0.001}_{-0.001}$	$-0.220^{+0.003}_{-0.003}$
$\langle I_{1c,i} \rangle, \langle I'_{1c,\perp} \rangle$	$0.671^{+0.004}_{-0.006}$	$0.253^{+0.005}_{-0.003}$	$0.615^{+0.005}_{-0.006}$	$0.343^{+0.004}_{-0.006}$	$0.549^{+0.006}_{-0.004}$	$0.294^{+0.005}_{-0.004}$	$0.503^{+0.004}_{-0.006}$	$0.377^{+0.004}_{-0.003}$	$0.504^{+0.005}_{-0.006}$	$0.376^{+0.004}_{-0.005}$	$0.572^{+0.006}_{-0.007}$	$0.326^{+0.005}_{-0.004}$
$\langle I_{2c,i} \rangle, \langle I'_{2c,\perp} \rangle$	$-0.632^{+0.005}_{-0.005}$	$0.083^{+0.004}_{-0.002}$	$-0.519^{+0.006}_{-0.007}$	$0.111^{+0.013}_{-0.010}$	$-0.632^{+0.005}_{-0.005}$	$0.096^{+0.007}_{-0.005}$	$-0.475^{+0.004}_{-0.008}$	$0.122^{+0.002}_{-0.001}$	$-0.476^{+0.005}_{-0.006}$	$0.119^{+0.004}_{-0.008}$	$-0.540^{+0.005}_{-0.006}$	$0.106^{+0.001}_{-0.001}$
$\langle I_{3,i} \rangle, \langle I'_{3,\perp} \rangle$	$-0.012^{+0.001}_{-0.001}$	$0.005^{+0.001}_{-0.001}$	$-0.017^{+0.001}_{-0.001}$	$0.007^{+0.000}_{-0.000}$	$-0.014^{+0.001}_{-0.001}$	$0.007^{+0.000}_{-0.000}$	$-0.004^{+0.001}_{-0.001}$	$0.001^{+0.001}_{-0.000}$	$-0.042^{+0.001}_{-0.001}$	$0.018^{+0.001}_{-0.001}$	$-0.016^{+0.001}_{-0.001}$	$0.007^{+0.000}_{-0.000}$
$\langle I_{4,i} \rangle, \langle I'_{4,\perp} \rangle$	$0.014^{+0.001}_{-0.001}$	$-0.020^{+0.001}_{-0.000}$	$0.022^{+0.001}_{-0.001}$	$-0.024^{+0.000}_{-0.000}$	$0.016^{+0.001}_{-0.001}$	$-0.008^{+0.001}_{-0.000}$	$0.008^{+0.000}_{-0.001}$	$-0.018^{+0.000}_{-0.000}$	$0.035^{+0.000}_{-0.001}$	$-0.030^{+0.000}_{-0.000}$	$0.019^{+0.001}_{-0.001}$	$-0.016^{+0.001}_{-0.000}$
$\langle I_{5,i} \rangle, \langle I'_{5,\perp} \rangle$	$0.188^{+0.021}_{-0.020}$	$-0.093^{+0.010}_{-0.010}$	$0.267^{+0.017}_{-0.017}$	$-0.123^{+0.011}_{-0.012}$	$0.226^{+0.019}_{-0.018}$	$-0.113^{+0.010}_{-0.009}$	$0.275^{+0.014}_{-0.017}$	$-0.135^{+0.010}_{-0.008}$	$0.261^{+0.019}_{-0.018}$	$-0.127^{+0.010}_{-0.009}$	$0.253^{+0.018}_{-0.016}$	$-0.126^{+0.009}_{-0.009}$
$\langle I_{6s,i} \rangle, \langle I'_{6s,\perp} \rangle$	$0.295^{+0.009}_{-0.010}$	$0.146^{+0.005}_{-0.005}$	$0.415^{+0.003}_{-0.004}$	$0.204^{+0.002}_{-0.002}$	$0.353^{+0.005}_{-0.006}$	$0.176^{+0.004}_{-0.004}$	$0.435^{+0.020}_{-0.020}$	$0.224^{+0.001}_{-0.001}$	$0.450^{+0.001}_{-0.001}$	$0.219^{+0.002}_{-0.002}$	$0.394^{+0.004}_{-0.005}$	$0.196^{+0.002}_{-0.002}$
$\langle I_{6c,i} \rangle, \langle I'_{6c,\perp} \rangle$	0	$0.292^{+0.010}_{-0.011}$	0	$0.407^{+0.004}_{-0.004}$	0	$0.353^{+0.007}_{-0.007}$	0	$0.449^{+0.002}_{-0.003}$	0	$0.439^{+0.003}_{-0.004}$	0	$0.391^{+0.005}_{-0.005}$



Table 18: Same as in Table 12, but for  $q^2 = [1.0 - 6.0]$  GeV<sup>2</sup> bin.

$q^2 = [1 - 6]$ GeV <sup>2</sup>												
Angular observables	SM		S1		S2		S3		S4		S5	
	$D_s\pi$	$D_s\gamma$	$D_s\pi$	$D_s\gamma$	$D_s\pi$	$D_s\gamma$	$D_s\pi$	$D_s\gamma$	$D_s\pi$	$D_s\gamma$	$D_s\pi$	$D_s\gamma$
$\langle I_{1s,0} \rangle, \langle I_{1s,\perp}^* \rangle$	$0.354^{+0.012}_{-0.012}$	$0.442^{+0.003}_{-0.002}$	$0.375^{+0.01}_{-0.010}$	$0.439^{+0.001}_{-0.001}$	$0.354^{+0.011}_{-0.011}$	$0.442^{+0.002}_{-0.002}$	$0.385^{+0.005}_{-0.006}$	$0.435^{+0.002}_{-0.002}$	$0.393^{+0.011}_{-0.010}$	$0.436^{+0.002}_{-0.002}$	$0.362^{+0.014}_{-0.006}$	$0.440^{+0.002}_{-0.002}$
$\langle I_{2s,0} \rangle, \langle I_{2s,\perp}^* \rangle$	$0.117^{+0.004}_{-0.004}$	$-0.199^{+0.011}_{-0.010}$	$0.124^{+0.004}_{-0.003}$	$-0.183^{+0.009}_{-0.008}$	$0.118^{+0.002}_{-0.004}$	$-0.200^{+0.010}_{-0.009}$	$0.128^{+0.007}_{-0.001}$	$-0.166^{+0.008}_{-0.010}$	$0.130^{+0.003}_{-0.002}$	$-0.165^{+0.009}_{-0.011}$	$0.120^{+0.005}_{-0.002}$	$-0.181^{+0.011}_{-0.010}$
$\langle I_{1c,0} \rangle, \langle I_{1c,\perp}^* \rangle$	$0.530^{+0.003}_{-0.002}$	$0.354^{+0.012}_{-0.012}$	$0.503^{+0.013}_{-0.014}$	$0.375^{+0.010}_{-0.010}$	$0.531^{+0.017}_{-0.015}$	$0.354^{+0.011}_{-0.011}$	$0.488^{+0.010}_{-0.015}$	$0.385^{+0.005}_{-0.006}$	$0.477^{+0.010}_{-0.014}$	$0.393^{+0.011}_{-0.010}$	$0.519^{+0.014}_{-0.019}$	$0.362^{+0.014}_{-0.006}$
$\langle I_{2c,0} \rangle, \langle I_{2c,\perp}^* \rangle$	$-0.518^{+0.015}_{-0.016}$	$0.117^{+0.004}_{-0.004}$	$-0.491^{+0.012}_{-0.013}$	$0.124^{+0.004}_{-0.003}$	$-0.518^{+0.017}_{-0.018}$	$0.118^{+0.002}_{-0.004}$	$-0.467^{+0.010}_{-0.017}$	$0.128^{+0.007}_{-0.001}$	$-0.466^{+0.010}_{-0.013}$	$0.130^{+0.003}_{-0.002}$	$-0.507^{+0.009}_{-0.018}$	$0.120^{+0.005}_{-0.002}$
$\langle I_{3,0} \rangle, \langle I_{3,\perp}^* \rangle$	$-0.006^{+0.008}_{-0.004}$	$0.003^{+0.001}_{-0.002}$	$-0.006^{+0.008}_{-0.004}$	$0.003^{+0.002}_{-0.001}$	$-0.006^{+0.008}_{-0.004}$	$0.004^{+0.002}_{-0.002}$	$-0.005^{+0.006}_{-0.003}$	$0.008^{+0.006}_{-0.006}$	$-0.015^{+0.006}_{-0.002}$	$0.007^{+0.004}_{-0.004}$	$-0.006^{+0.008}_{-0.004}$	$0.005^{+0.007}_{-0.004}$
$\langle I_{4,0} \rangle, \langle I_{4,\perp}^* \rangle$	$0.210^{+0.004}_{-0.004}$	$-0.105^{+0.002}_{-0.002}$	$0.205^{+0.004}_{-0.003}$	$-0.103^{+0.002}_{-0.002}$	$0.200^{+0.004}_{-0.004}$	$-0.100^{+0.002}_{-0.002}$	$0.181^{+0.004}_{-0.004}$	$-0.095^{+0.002}_{-0.002}$	$0.205^{+0.005}_{-0.005}$	$-0.100^{+0.002}_{-0.002}$	$0.244^{+0.009}_{-0.010}$	$-0.101^{+0.010}_{-0.002}$
$\langle I_{5,0} \rangle, \langle I_{5,\perp}^* \rangle$	$-0.127^{+0.017}_{-0.020}$	$0.064^{+0.008}_{-0.010}$	$-0.065^{+0.019}_{-0.023}$	$0.034^{+0.008}_{-0.012}$	$-0.106^{+0.018}_{-0.022}$	$0.053^{+0.009}_{-0.011}$	$-0.048^{+0.022}_{-0.019}$	$0.025^{+0.010}_{-0.009}$	$-0.099^{+0.021}_{-0.020}$	$0.046^{+0.010}_{-0.012}$	$-0.083^{+0.017}_{-0.023}$	$0.040^{+0.010}_{-0.011}$
$\langle I_{6s,0} \rangle, \langle I_{6s,\perp}^* \rangle$	$-0.315^{+0.042}_{-0.283}$	$-0.153^{+0.013}_{-0.016}$	$-0.173^{+0.204}_{-0.139}$	$-0.082^{+0.014}_{-0.018}$	$-0.258^{+0.087}_{-0.225}$	$-0.129^{+0.015}_{-0.016}$	$-0.421^{+0.174}_{-0.110}$	$-0.067^{+0.015}_{-0.015}$	$-0.152^{+0.083}_{-0.18}$	$-0.071^{+0.015}_{-0.016}$	$-0.205^{+0.035}_{-0.172}$	$-0.100^{+0.015}_{-0.016}$
$\langle I_{6c,0} \rangle, \langle I_{6c,\perp}^* \rangle$	0	$-0.306^{+0.027}_{-0.031}$	0	$-0.163^{+0.029}_{-0.032}$	0	$-0.258^{+0.029}_{-0.033}$	0	$-0.135^{+0.028}_{-0.08}$	0	$-0.142^{+0.029}_{-0.032}$	0	$-0.200^{+0.030}_{-0.0335}$

## References

- [1] **LHCb** Collaboration, R. Aaij et al., *Angular analysis of the  $B^0 \rightarrow K^{*0} \mu^+ \mu^-$  decay using  $3 \text{ fb}^{-1}$  of integrated luminosity*, *JHEP* **02** (2016) 104, [[arXiv:1512.04442](#)].
- [2] **LHCb** Collaboration, R. Aaij et al., *Measurement of CP-Averaged Observables in the  $B^0 \rightarrow K^{*0} \mu^+ \mu^-$  Decay*, *Phys. Rev. Lett.* **125** (2020), no. 1 011802, [[arXiv:2003.04831](#)].
- [3] **LHCb** Collaboration, R. Aaij et al., *Angular Analysis of the  $B^+ \rightarrow K^{*+} \mu^+ \mu^-$  Decay*, *Phys. Rev. Lett.* **126** (2021), no. 16 161802, [[arXiv:2012.13241](#)].
- [4] **CMS** Collaboration, A. M. Sirunyan et al., *Angular analysis of the decay  $B^+ \rightarrow K^*(892)^+ \mu^+ \mu^-$  in proton-proton collisions at  $\sqrt{s} = 8 \text{ TeV}$* , *JHEP* **04** (2021) 124, [[arXiv:2010.13968](#)].
- [5] **LHCb** Collaboration, R. Aaij et al., *Angular analysis of charged and neutral  $B \rightarrow K \mu^+ \mu^-$  decays*, *JHEP* **05** (2014) 082, [[arXiv:1403.8045](#)].
- [6] **LHCb** Collaboration, R. Aaij et al., *Measurement of the phase difference between short- and long-distance amplitudes in the  $B^+ \rightarrow K^+ \mu^+ \mu^-$  decay*, *Eur. Phys. J. C* **77** (2017), no. 3 161, [[arXiv:1612.06764](#)].
- [7] **CMS** Collaboration, A. M. Sirunyan et al., *Angular analysis of the decay  $B^+ \rightarrow K^+ \mu^+ \mu^-$  in proton-proton collisions at  $\sqrt{s} = 8 \text{ TeV}$* , *Phys. Rev. D* **98** (2018), no. 11 112011, [[arXiv:1806.00636](#)].
- [8] D. Becirevic and E. Schneider, *On transverse asymmetries in  $B \rightarrow K^* \ell^+ \ell^-$* , *Nucl. Phys. B* **854** (2012) 321–339, [[arXiv:1106.3283](#)].
- [9] M. Ciuchini, M. Fedele, E. Franco, S. Mishima, A. Paul, L. Silvestrini, and M. Valli,  *$B \rightarrow K^* \ell^+ \ell^-$  decays at large recoil in the Standard Model: a theoretical reappraisal*, *JHEP* **06** (2016) 116, [[arXiv:1512.07157](#)].
- [10] G. Hiller and F. Kruger, *More model-independent analysis of  $b \rightarrow s$  processes*, *Phys. Rev. D* **69** (2004) 074020, [[hep-ph/0310219](#)].
- [11] **LHCb** Collaboration, *Test of lepton universality in  $b \rightarrow s \ell^+ \ell^-$  decays*, [[arXiv:2212.09152](#)].
- [12] **LHCb** Collaboration, *Measurement of lepton universality parameters in  $B^+ \rightarrow K^+ \ell^+ \ell^-$  and  $B^0 \rightarrow K^{*0} \ell^+ \ell^-$  decays*, [[arXiv:2212.09153](#)].
- [13] **LHCb** Collaboration, R. Aaij et al., *Differential branching fractions and isospin asymmetries of  $B \rightarrow K^{(*)} \mu^+ \mu^-$  decays*, *JHEP* **06** (2014) 133, [[arXiv:1403.8044](#)].
- [14] **LHCb** Collaboration, R. Aaij et al., *Differential branching fraction and angular analysis of the decay  $B^0 \rightarrow K^{*0} \mu^+ \mu^-$* , *JHEP* **08** (2013) 131, [[arXiv:1304.6325](#)].
- [15] **LHCb** Collaboration, R. Aaij et al., *Measurements of the S-wave fraction in  $B^0 \rightarrow K^+ \pi^- \mu^+ \mu^-$  decays and the  $B^0 \rightarrow K^*(892)^0 \mu^+ \mu^-$  differential branching fraction*, *JHEP* **11** (2016) 047, [[arXiv:1606.04731](#)]. [Erratum: *JHEP* **04**, 142 (2017)].
- [16] **LHCb** Collaboration, R. Aaij et al., *Differential branching fraction and angular analysis of the decay  $B_s^0 \rightarrow \phi \mu^+ \mu^-$* , *JHEP* **07** (2013) 084, [[arXiv:1305.2168](#)].

- [17] **LHCb** Collaboration, R. Aaij et al., *Angular analysis and differential branching fraction of the decay  $B_s^0 \rightarrow \phi \mu^+ \mu^-$* , *JHEP* **09** (2015) 179, [[arXiv:1506.08777](#)].
- [18] S. Descotes-Genon, J. Matias, M. Ramon, and J. Virto, *Implications from clean observables for the binned analysis of  $B \rightarrow K^* \mu^+ \mu^-$  at large recoil*, *JHEP* **01** (2013) 048, [[arXiv:1207.2753](#)].
- [19] S. Descotes-Genon, T. Hurth, J. Matias, and J. Virto, *Optimizing the basis of  $B \rightarrow K^* \ell \ell$  observables in the full kinematic range*, *JHEP* **05** (2013) 137, [[arXiv:1303.5794](#)].
- [20] **ATLAS** Collaboration, M. Aaboud et al., *Angular analysis of  $B_d^0 \rightarrow K^* \mu^+ \mu^-$  decays in  $pp$  collisions at  $\sqrt{s} = 8$  TeV with the ATLAS detector*, *JHEP* **10** (2018) 047, [[arXiv:1805.04000](#)].
- [21] J. Aebischer, J. Kumar, P. Stangl, and D. M. Straub, *A Global Likelihood for Precision Constraints and Flavour Anomalies*, *Eur. Phys. J. C* **79** (2019), no. 6 509, [[arXiv:1810.07698](#)].
- [22] **Belle** Collaboration, A. Abdesselam et al., *Angular analysis of  $B^0 \rightarrow K^*(892)^0 \ell^+ \ell^-$* , in *LHC Ski 2016: A First Discussion of 13 TeV Results*, 4, 2016. [[arXiv:1604.04042](#)].
- [23] **Belle** Collaboration, S. Wehle et al., *Lepton-Flavor-Dependent Angular Analysis of  $B \rightarrow K^* \ell^+ \ell^-$* , *Phys. Rev. Lett.* **118** (2017), no. 11 111801, [[arXiv:1612.05014](#)].
- [24] **CMS** Collaboration, A. M. Sirunyan et al., *Measurement of angular parameters from the decay  $B^0 \rightarrow K^{*0} \mu^+ \mu^-$  in proton-proton collisions at  $\sqrt{s} = 8$  TeV*, *Phys. Lett. B* **781** (2018) 517–541, [[arXiv:1710.02846](#)].
- [25] M. Algueró, B. Capdevila, S. Descotes-Genon, J. Matias, and M. Novoa-Brunet,  *$b \rightarrow s \ell \ell$  global fits after Moriond 2021 results*, in *55th Rencontres de Moriond on QCD and High Energy Interactions*, 4, 2021. [[arXiv:2104.08921](#)].
- [26] S. Descotes-Genon, L. Hofer, J. Matias, and J. Virto, *Global analysis of  $b \rightarrow s \ell \ell$  anomalies*, *JHEP* **06** (2016) 092, [[arXiv:1510.04239](#)].
- [27] W. Altmannshofer, C. Niehoff, P. Stangl, and D. M. Straub, *Status of the  $B \rightarrow K^* \mu^+ \mu^-$  anomaly after Moriond 2017*, *Eur. Phys. J. C* **77** (2017), no. 6 377, [[arXiv:1703.09189](#)].
- [28] A. K. Alok, B. Bhattacharya, A. Datta, D. Kumar, J. Kumar, and D. London, *New Physics in  $b \rightarrow s \mu^+ \mu^-$  after the Measurement of  $R_{K^*}$* , *Phys. Rev.* **D96** (2017), no. 9 095009, [[arXiv:1704.07397](#)].
- [29] W. Altmannshofer, P. Stangl, and D. M. Straub, *Interpreting Hints for Lepton Flavor Universality Violation*, *Phys. Rev.* **D96** (2017), no. 5 055008, [[arXiv:1704.05435](#)].
- [30] L.-S. Geng, B. Grinstein, S. Jäger, J. Martin Camalich, X.-L. Ren, and R.-X. Shi, *Towards the discovery of new physics with lepton-universality ratios of  $b \rightarrow s \ell \ell$  decays*, *Phys. Rev.* **D96** (2017), no. 9 093006, [[arXiv:1704.05446](#)].
- [31] M. Ciuchini, A. M. Coutinho, M. Fedele, E. Franco, A. Paul, L. Silvestrini, and M. Valli, *On Flavourful Easter eggs for New Physics hunger and Lepton Flavour Universality violation*, *Eur. Phys. J. C* **77** (2017), no. 10 688, [[arXiv:1704.05447](#)].

- [32] B. Capdevila, A. Crivellin, S. Descotes-Genon, J. Matias, and J. Virto, *Patterns of New Physics in  $b \rightarrow sl^+\ell^-$  transitions in the light of recent data*, *JHEP* **01** (2018) 093, [[arXiv:1704.05340](#)].
- [33] M. Algueró, B. Capdevila, A. Crivellin, S. Descotes-Genon, P. Masjuan, J. Matias, M. Novoa Brunet, and J. Virto, *Emerging patterns of New Physics with and without Lepton Flavour Universal contributions*, *Eur. Phys. J.* **C79** (2019), no. 8 714, [[arXiv:1903.09578](#)]. [Addendum: *Eur.Phys.J.C* 80, 511 (2020)].
- [34] A. K. Alok, A. Dighe, S. Gangal, and D. Kumar, *Continuing search for new physics in  $b \rightarrow s\mu\mu$  decays: two operators at a time*, *JHEP* **06** (2019) 089, [[arXiv:1903.09617](#)].
- [35] M. Ciuchini, A. M. Coutinho, M. Fedele, E. Franco, A. Paul, L. Silvestrini, and M. Valli, *New Physics in  $b \rightarrow sl^+\ell^-$  confronts new data on Lepton Universality*, *Eur. Phys. J.* **C79** (2019), no. 8 719, [[arXiv:1903.09632](#)].
- [36] A. Datta, J. Kumar, and D. London, *The  $B$  anomalies and new physics in  $b \rightarrow se^+e^-$* , *Phys. Lett.* **B797** (2019) 134858, [[arXiv:1903.10086](#)].
- [37] J. Aebischer, W. Altmannshofer, D. Guadagnoli, M. Reboud, P. Stangl, and D. M. Straub,  *$B$ -decay discrepancies after Moriond 2019*, *Eur. Phys. J. C* **80** (2020), no. 3 252, [[arXiv:1903.10434](#)].
- [38] K. Kowalska, D. Kumar, and E. M. Sessolo, *Implications for new physics in  $b \rightarrow s\mu\mu$  transitions after recent measurements by Belle and LHCb*, *Eur. Phys. J.* **C79** (2019), no. 10 840, [[arXiv:1903.10932](#)].
- [39] A. Arbey, T. Hurth, F. Mahmoudi, D. M. Santos, and S. Neshatpour, *Update on the  $b \rightarrow s$  anomalies*, *Phys. Rev.* **D100** (2019), no. 1 015045, [[arXiv:1904.08399](#)].
- [40] S. Bhattacharya, A. Biswas, S. Nandi, and S. K. Patra, *Exhaustive model selection in  $b \rightarrow sll$  decays: Pitting cross-validation against the Akaike information criterion*, *Phys. Rev. D* **101** (2020), no. 5 055025, [[arXiv:1908.04835](#)].
- [41] A. Biswas, S. Nandi, S. K. Patra, and I. Ray, *New physics in  $b \rightarrow sll$  decays with complex Wilson coefficients*, *Nucl. Phys. B* **969** (2021) 115479, [[arXiv:2004.14687](#)].
- [42] A. K. Alok, N. R. Singh Chundawat, S. Gangal, and D. Kumar, *A global analysis of  $b \rightarrow sll$  data in heavy and light  $Z'$  models*, *Eur. Phys. J. C* **82** (2022), no. 10 967, [[arXiv:2203.13217](#)].
- [43] Z.-R. Huang, M. A. Paracha, I. Ahmed, and C.-D. Lü, *Testing Leptoquark and  $Z'$  Models via  $B \rightarrow K_1(1270, 1400)\mu^+\mu^-$  Decays*, *Phys. Rev. D* **100** (2019), no. 5 055038, [[arXiv:1812.03491](#)].
- [44] F. Munir Bhutta, Z.-R. Huang, C.-D. Lü, M. A. Paracha, and W. Wang, *New physics in  $b \rightarrow sll$  anomalies and its implications for the complementary neutral current decays*, *Nucl. Phys. B* **979** (2022) 115763, [[arXiv:2009.03588](#)].
- [45] D. Das, B. Kindra, G. Kumar, and N. Mahajan,  *$B \rightarrow K_2^*(1430)\ell^+\ell^-$  distributions at large recoil in the Standard Model and beyond*, *Phys. Rev. D* **99** (2019), no. 9 093012, [[arXiv:1812.11803](#)].



- [46] M. K. Mohapatra and A. Giri, *Implications of light  $Z'$  on semileptonic  $B(B_s) \rightarrow T\{K_2^*(1430)(f_2'(1525))\}\ell^+\ell^-$  decays at large recoil*, *Phys. Rev. D* **104** (2021), no. 9 095012, [[arXiv:2109.12382](#)].
- [47] N. Rajeev, N. Sahoo, and R. Dutta, *Angular analysis of  $B_s \rightarrow f_2'(1525) (\rightarrow K^+ K^-) \mu^+ \mu^-$  decays as a probe to lepton flavor universality violation*, *Phys. Rev. D* **103** (2021), no. 9 095007, [[arXiv:2009.06213](#)].
- [48] R. Dutta, *Model independent analysis of new physics effects on  $B_c \rightarrow (D_s, D_s^*) \mu^+ \mu^-$  decay observables*, *Phys. Rev. D* **100** (2019), no. 7 075025, [[arXiv:1906.02412](#)].
- [49] M. K. Mohapatra, N. Rajeev, and R. Dutta, *Combined analysis of  $B_c \rightarrow D_s^{(*)} \mu^+ \mu^-$  and  $B_c \rightarrow D_s^{(*)} \nu \bar{\nu}$  decays within  $Z'$  and leptoquark new physics models*, *Phys. Rev. D* **105** (2022), no. 11 115022, [[arXiv:2108.10106](#)].
- [50] A. Paul and D. M. Straub, *Constraints on new physics from radiative  $B$  decays*, *JHEP* **04** (2017) 027, [[arXiv:1608.02556](#)].
- [51] C. Bobeth, M. Misiak, and J. Urban, *Photonic penguins at two loops and  $m_t$  dependence of  $BR[B \rightarrow X_s l^+ l^-]$* , *Nucl. Phys. B* **574** (2000) 291–330, [[hep-ph/9910220](#)].
- [52] M. Beneke, T. Feldmann, and D. Seidel, *Systematic approach to exclusive  $B \rightarrow V l^+ l^-$ ,  $V \gamma$  decays*, *Nucl. Phys.* **B612** (2001) 25–58, [[hep-ph/0106067](#)].
- [53] H. H. Asatrian, H. M. Asatrian, C. Greub, and M. Walker, *Two loop virtual corrections to  $B \rightarrow X_s l^+ l^-$  in the standard model*, *Phys. Lett. B* **507** (2001) 162–172, [[hep-ph/0103087](#)].
- [54] H. H. Asatryan, H. M. Asatrian, C. Greub, and M. Walker, *Calculation of two loop virtual corrections to  $b \rightarrow s l^+ l^-$  in the standard model*, *Phys. Rev.* **D65** (2002) 074004, [[hep-ph/0109140](#)].
- [55] C. Greub, V. Pilipp, and C. Schupbach, *Analytic calculation of two-loop QCD corrections to  $b \rightarrow s l^+ l^-$  in the high  $q^2$  region*, *JHEP* **12** (2008) 040, [[arXiv:0810.4077](#)].
- [56] D. Du, A. X. El-Khadra, S. Gottlieb, A. S. Kronfeld, J. Laiho, E. Lunghi, R. S. Van de Water, and R. Zhou, *Phenomenology of semileptonic  $B$ -meson decays with form factors from lattice QCD*, *Phys. Rev.* **D93** (2016), no. 3 034005, [[arXiv:1510.02349](#)].
- [57] A. Faessler, T. Gutsche, M. A. Ivanov, J. G. Korner, and V. E. Lyubovitskij, *The Exclusive rare decays  $B \rightarrow K(K^*) \bar{\ell} \ell$  and  $B_c \rightarrow D(D^*) \bar{\ell} \ell$  in a relativistic quark model*, *Eur. Phys. J. direct* **4** (2002), no. 1 18, [[hep-ph/0205287](#)].
- [58] D. Ebert, R. N. Faustov, and V. O. Galkin, *Rare Semileptonic Decays of  $B$  and  $B_c$  Mesons in the Relativistic Quark Model*, *Phys. Rev. D* **82** (2010) 034032, [[arXiv:1006.4231](#)].
- [59] D. Ebert, R. N. Faustov, and V. O. Galkin, *Form-factors of heavy to light  $B$  decays at large recoil*, *Phys. Rev. D* **64** (2001) 094022, [[hep-ph/0107065](#)].
- [60] **Particle Data Group** Collaboration, R. L. Workman et al., *Review of Particle Physics*, *PTEP* **2022** (2022) 083C01.
- [61] T. Blake, G. Lanfranchi, and D. M. Straub, *Rare  $B$  Decays as Tests of the Standard Model*, *Prog. Part. Nucl. Phys.* **92** (2017) 50–91, [[arXiv:1606.00916](#)].